AD_____

Award Number: W81XWH-04-1-0570

TITLE: Endocrine Therapy of Breast Cancer

PRINCIPAL INVESTIGATOR: Robert S. Clarke, Ph.D.

CONTRACTING ORGANIZATION: Georgetown University
Washington, DC 20057

REPORT DATE: June 2005

TYPE OF REPORT: Annual

PREPARED FOR: U.S. Army Medical Research and Materiel Command
Fort Detrick, Maryland 21702-5012

DISTRIBUTION STATEMENT: Approved for Public Release;
Distribution Unlimited

REPORT DOCUMENTATION PAGE

Form Approved
OMB No. 0704-0188

1. REPORT DATE *(DD-MM-YYYY)*	2. REPORT TYPE	3. DATES COVERED *(From - To)*
01-06-2005	Annual	17 May 2004 – 16 May 2005

4. TITLE AND SUBTITLE
Endocrine Therapy of Breast Cancer

5a. CONTRACT NUMBER

5b. GRANT NUMBER
W81XWH-04-1-0570

5c. PROGRAM ELEMENT NUMBER

6. AUTHOR(S)
Robert S. Clarke, Ph.D.

E-mail: a36@psu.edu

5d. PROJECT NUMBER

5e. TASK NUMBER

5f. WORK UNIT NUMBER

7. PERFORMING ORGANIZATION NAME(S) AND ADDRESS(ES)

Georgetown University
Washington, DC 20057

8. PERFORMING ORGANIZATION REPORT NUMBER

9. SPONSORING / MONITORING AGENCY NAME(S) AND ADDRESS(ES)
U.S. Army Medical Research and Materiel Command
Fort Detrick, Maryland 21702-5012

10. SPONSOR/MONITOR'S ACRONYM(S)

11. SPONSOR/MONITOR'S REPORT NUMBER(S)

12. DISTRIBUTION / AVAILABILITY STATEMENT
Approved for Public Release; Distribution Unlimited

13. SUPPLEMENTARY NOTES

14. ABSTRACT

A recent controversy in the treatment of estrogen receptor positive (ER+) breast cancers is whether an aromatase inhibitor, *e.g.,* letrozole (LET) or TAM should be given as first line endocrine therapy. Unfortunately, response rates are lower, and response durations are shorter, on crossover than when these agents are given as first line therapies, *e.g.,* ~40% of tumors show crossresistance to TAM or an aromatase inhibitor on crossover. Only 50% of ER+ tumors respond to endocrine therapy. Currently, we fail to predict endocrine responsiveness in about 66% of ER+/PgR- (progesterone receptor), 55% of ER-/PgR+, and 25% of ER+/PgR+ tumors. In this new Clinical Translational Research Award, we hypothesize that our analytical methods can extract expression profiles of breast tumors that define their responsiveness (sensitive *vs.* resistant) to endocrine therapy. These profiles, when combined with known predictive/prognostic factors, will support neural network and biostatistical classifiers or committee machines that predict each tumor's endocrine responsiveness. Our objectives are to array breast cancer cases, build classifiers of endocrine responsiveness (using microarray data), and validate these classifiers in independent data sets using mostly immunohistochemistry data (IHC). IHC will be done on cases with definitive outcomes data. In the long term, we will design custom arrays for use in clinical practice. Genes will be further studied using cellular and molecular methods, and their role as therapeutic targets explored.

15. SUBJECT TERMS Antiestrogen, aromatase inhibitor, anastrazole, bioinformatics, biomarkers, biostatistics, breast cancer, class prediction, clinical trial, computer science, engineering, immunohistochemistry, letrozole, microarrays, molecular profiling, neural networks, recurrence, resistance, tamoxifen

16. SECURITY CLASSIFICATION OF:			17. LIMITATION OF ABSTRACT	18. NUMBER OF PAGES	19a. NAME OF RESPONSIBLE PERSON
a. REPORT	b. ABSTRACT	c. THIS PAGE			19b. TELEPHONE NUMBER *(include area code)*
U	U	U	UU	39	

TABLE OF CONTENTS

1. Wang, Y., Wang, Z., Xuan, J., Zhang, J., Hoffman, E.P., Clarke, R. & Khan, J. "Optimizing multilayer perceptrons by discriminatory component analysis." Proc IEEE Workshops Machine Learn Signal Process, Sao Luis, Brazil, pp. 273-282, 2004.

2. Bouker, K.B., Skaar, T.C., Fernandez, D.R., O'Brien, K.A., Riggins, R.B., Honghua, C. & Clarke, R. "Interferon regulatory factor-1 mediates the proapoptotic but not cell cycle arrest effects of the steroidal antiestrogen ICI 182,780 (Faslodex, Fulvestrant)." Cancer Res, 64:4030-4039, 2004.

3. Riggins, R.B., Nehra, R., Zwart, A., Agarwal, P. & Clarke, R. "The NFκB inhibitor parthenolide restores ICI 182,780 (Faslodex; Fulvestrant)-induced apoptosis in antiestrogen resistant breast cancer cells." Mol Cancer Ther, 4: 323-412, 2005.

INTRODUCTION

Endocrine therapy is often the least toxic and most effective treatment for hormone receptor positive invasive breast cancer. Such therapy includes antiestrogens (tamoxifen, fulvestrant) and aromatase inhibitors (anastrozole, letrozole, exemestane). Tamoxifen (TAM) increases disease free and overall survival in the adjuvant setting, reduces the incidence of estrogen receptor positive disease (ER+; unless otherwise noted ER=ERα) in high-risk women, and reduces the rate of bone loss secondary to osteoporosis in postmenopausal women [1,2]. Aromatase inhibitors are effective only in the absence of functioning ovaries - TAM can be used regardless of menopausal status. Recent studies suggest that anastrozole may be superior to TAM in the adjuvant treatment of postmenopausal women with ER+ breast cancer; other studies report higher overall response rates with letrozole (LET) *vs.* TAM as first line therapy in the metastatic setting. Thus, a recent controversy in the management of patients with ER+ disease is whether an aromatase inhibitor or TAM should be given as first line endocrine therapy [3-9].

In this new Clinical Translational Research award, we will build classifiers that accurately separate antiestrogen sensitive from antiestrogen resistant breast tumors and begin to assist in the direction of specific endocrine treatments (antiestrogen *vs.* aromatase inhibitor) to *individual* patients. We hypothesize that endocrine responsiveness is affected by a gene network, rather than the activity of only one or two genes or signaling pathways [10-12]. Since the key components of such a network are unknown, we must study 10,000s of genes. We will use Affymetrix GeneChips. We will not identify mutational events, the presence of mRNA splice variants, or post-translational protein modifications. However, these factors have major effects on the transcriptome and their "footprints" should be identified by expression microarrays.

BODY

Overview: We will build classifiers that separate antiestrogen sensitive from antiestrogen resistant breast tumors and begin to assist in the direction of specific endocrine treatments (antiestrogen *vs.* aromatase inhibitor) to *individual* patients. To achieve this goal, and consistent with a CTR award, we will complete a 4-year, prospective, neoadjuvant study with Letrozole (LET) or TAM as the only systemic therapy. We will obtain molecular profiles from Affymetrix GeneChips and further develop and apply our innovative bioinformatic and biostatistic methods to explore these high dimensional data sets and build/validate new classifiers. A more accurate predictor of endocrine responsiveness would have widespread clinical use, allowing women and physicians to make more individualized and appropriate treatment decisions. For example, patients with tumors predicted to be resistant to antiestrogens and/or aromatase inhibitors would be strong candidates for an early intervention with cytotoxic chemotherapy.

In most predictive/prognostic marker studies investigators focus on a *single* factor and whether they obtain a p-value that reaches conventional statistical significance. Our approach is different because we will determine whether we can find joint gene subsets that can separate patients into sufficiently distinct groups that should differ in their treatment. We will **(1)** analyze >33,000 genes on retrospective and prospective material, **(2)** apply new biostatistical and bioinformatic methods to identify ~40 potentially informative "biomarkers," **(3)** build neural network and biostatistical model classifiers, **(4)** evaluate the joint discriminant power of selected genes concurrently rather than as single biomarkers, **(5)** focus on prediction for individual patients where the assessment of a p-value is less important than the classification rate of our predictors, **(6)** validate the classifiers in independent data sets, and **(7)** explore the ability of predictors to refine the targeting of *specific* endocrine therapies.

Evidence has begun to accumulate suggesting that an aromatase inhibitor might be a more effective first line endocrine therapy for some breast cancer patients than the current standard of care (Tamoxifen). These data have generated considerable interest and controversy, in part because unlike TAM, there are no long term studies with aromatase inhibitors where definitive survival data are available. Our study could provide new and innovative insights into how to approach the more effective targeting of specific endocrine therapies to individual patients.

Specific Aims (from the original application)
We will complete two clinical studies and collect gene expression profiles from which to build predictors of endocrine responsiveness. Predictors will be built in Specific Aim 2 and validated in Specific Aim 3.

AIM 1: Clinical Studies - **Clinical Study-1** (retrospective) is of pretreatment, single, frozen samples where we will compare the molecular profiles of tumors that recurred on TAM with those of tumors that did not recur. Each resistant sample is matched with a TAM sensitive sample by age, stage, and duration of follow-up. We also have further, single (unmatched), frozen samples from patients already progressing on TAM. **Clinical Study-2** is a prospective study of breast tumor samples from patients treated with neoadjuvant TAM or LET.

AIM 2: We will develop and apply novel bioinformatics and biostatistics to discover gene subsets that define the molecular differences between endocrine sensitive and resistant breast tumors. These genes will be used, in combination with established predictive/prognostic factors, *e.g.,* ER, PgR, stage, to build innovative classifiers that can better predict an individual tumor's endocrine responsiveness.

AIM 3: We will test, optimize, and validate the performance of the classifiers from Aim 2 in retrospective studies of human breast tumors. We will measure each gene individually by IHC, *in situ* RNA hybridization (ISH), or *real time* PCR (RT-PCR).

KEY RESEARCH ACCOMPLISHMENTS

Progress on the clinical goals for Year-1 was greatly delayed because of the time taken to obtain DOD approval of our preexisting institutionally approved IRBs at Georgetown University and at the University of Edinburgh. All institutionally approved protocols and requested material were submitted to the DOD in July 2004; additional information, requested by the DOD several months later, was submitted in November 2004. We did not receive final approval to proceed with the clinical studies until March 2005. Much of this delay seems to have been unavoidable and due, in part, to personnel changes at the DOD (within USAMRMC). While this has likely left us behind schedule in recruitment to the prospective studies, we were able to proceed with the informatics (algorithm development and optimization) and infrastructure development (database development and installation). We also used this time to obtain retrospective material from the University of Edinburgh (we obtained, annotated, and stored this material but could not use the samples until we had formal final approval from the DOD), and to further optimize our microarray procedures and complete modifications to our standard operating procedure documents. We also completed some of the studies presented in our preliminary data and submitted these for publication. The *in silico* tissue heterogeneity correction method described in the application was developed sufficiently and submitted for publication – this was sent out for review by Nature Methods but we do not know the final outcome. Publications supported since this award are listed under "Reportable Outcomes" (below) and constitute some of our major accomplishments in the first year.

Other key research accomplishments are related to the goals set towards the establishment of our Center application; these are more closely related to the Statement of Work and are presented in this context below.

Statement of Work (from the original application)

- **TASK 1.** Array breast tumor samples from Clinical Studies 1 (retrospective) and 2 (prospective): (1-48 Months)

To perform this task we will obtain breast tumor samples and clinical information from University of Edinburgh, collect and quality test RNA using validated tissue acquisition and processing protocol, and array RNA samples on oligonucleotide chips (*i.e.,* U133A Affymetrix GeneChips). ***Please note that we originally described analyses of approximately 12,000 genes in each sample and now indicate that we will measure***

almost 3-times as many genes. The increase is possible because Affymetrix improved their technology and now produce single chips with 40,000 probe sets representing 39,000 transcripts, of which 33,000 are well-substantiated genes. The cost of these chips, which essentially represent the probe sets previously included on two chips (U133A and U133B), is the same as the original U133A GeneChips described when the application was submitted. Since we were unable to start arraying in year 1 (see below), this proved very fortunate, since it greatly increases the power of our study to detect meaningful predictive patterns and genes or networks associated with the clinical outcomes.

We have recently begun extracting and assessing RNA from the samples we have received to date. If the high quality of the initial specimens is apparent in subsequent material, we should be able to start arraying the retrospectively collected material within the next few months. Thus, we would hope to remain on track in Year 2 and begin generating our first series of data for analysis.

Note: minor change to SOW – we will use the Affymetrix U133 Plus 2.0 GeneChips (not U133A).

- **TASK 2.** Store, process, and train/optimize classifiers from gene expression microarray data: (1-48 Months)

To perform this task we will modify MIAME Compliant DSAD Database that can be readily exported to National Cancer Institute Center for Bioinformatics. We will submit collected de-identified clinical information into the DSAD database and process gene expression data with "in house" state-of-the-art algorithms (we will also further develop and optimize these algorithms throughout this award period). For the initial studies we will train/optimize initial neural network RNA classifier (MLP), the final classifier for the microarray data will be built when we have completed arraying all samples.

We have made significant progress on addressing this task and are likely ahead of schedule, largely as a consequence of our involvement in the National Cancer Institute Center for Bioinformatics (NCICB) caBIG project. The PI (Dr. Clarke) leads the Lombardi Comprehensive Cancer Center's caBIG team and we have been actively involved in the development of caArray (NCICB's grid-enabled, MIAME compliant, microarray database). We chose to adopt this database, rather than continue working on our own DSAD, because caArray is further developed and already has most of the functions we require. We now have a working installation of caArray and are already able to store and exchange microarray data in our testing of this system. The caBIG program is open source-open access and is widely supported by NCICB and teams of collaborating scientists at other Cancer Centers across the country. We also have found the NCICB team highly responsive when we identify bugs or problems with the software. We anticipate that continued collaboration through the caBIG community will prove a more cost and time efficient approach to developing some components of the research infrastructure described in the original application. It is our intent to build any additional components in a manner consistent with the guidelines established by the caBIG community, since this will likely ensure long term viability and compatibility of our database structure.

Note: minor change to SOW - we will now use the caArray database rather than the DSAD as we initially proposed.

- **TASK 3.** Retrain/reoptimize classifiers using IHC data from Series 1 (Archival Tissues) and Series 2 (Scottish Adjuvant TAM Trial) for Validation: (Months 24-48):

To perform this task we will obtain clinical information and breast tumor samples from the University of Edinburgh (formalin fixed/paraffin embedded). We will rank and prioritize selected joint genes from RNA classifiers built and optimized in TASK 2 (above) and retrain/reoptimize the initial neural network IHC

classifier (MLP). Finally, we will validate IHC classifier on independent data sets (data sets not used to build and train the MLP classifiers).

We will not be able to start this task on the timeframe as initially proposed here because of the delays in getting approval to work with the clinical specimens. However, we hope to be able to recover time in the coming 12 months and still finish these tasks within the period of funding. We have completed the preliminary data on the use of IHC and tissue microarrays to explore an initial gene set implicated in antiestrogen resistance. We also have performed and published initial mechanistic studies on some of these genes, consistent with the goals of Task 3, since we anticipate obtaining additional data further implicating these genes in Task 1.

REPORTABLE OUTCOMES

Papers and Meeting Reports*

- Wang, Y., Wang, Z., Xuan, J., Zhang, J., Hoffman, E.P., Clarke, R. & Khan, J. "Optimizing multilayer perceptrons by discriminatory component analysis." Proc IEEE Workshops Machine Learn Signal Process, Sao Luis, Brazil, pp. 273-282, 2004.

- Bouker, K.B., Skaar, T.C., Fernandez, D.R., O'Brien, K.A., Riggins, R.B., Honghua, C. & Clarke, R. "Interferon regulatory factor-1 mediates the proapoptotic but not cell cycle arrest effects of the steroidal antiestrogen ICI 182,780 (Faslodex, Fulvestrant)." Cancer Res, 64:4030-4039, 2004.

- Riggins, R.B., Nehra, R., Zwart, A., Agarwal, P. & Clarke, R. "The NFκB inhibitor parthenolide restores ICI 182,780 (Faslodex; Fulvestrant)-induced apoptosis in antiestrogen resistant breast cancer cells." Mol Cancer Ther, 4: 323-412, 2005.

- Zhu, Y., Singh, B., Hewitt, S., Liu, A., Gomez, B., Wang, A. & Clarke, R. "Expression patterns among proteins associated with endocrine responsiveness in breast cancer: interferon regulatory factor-1, human X-box binding protein-1, nuclear factor kappa B, nucleophosmin, estrogen receptor-alpha, and progesterone receptor." Int J Oncol, in press.

- Xuan, J., Dong, Y., Khan, J., Hoffman, E., Clarke, R. & Wang, Y. "Robust feature selection by weighted Fisher criterion for multiclass prediction in gene expression profiling." Proc Intl Conf Pattern Recon, in press.

- Riggins, R.B., Bouton, A.H., Liu, M.C. & Clarke, R. "Antiestrogens, aromatase inhibitors, and apoptosis in breast cancer." Vit Horm, in press.

- Bouker, K.B., Skaar, T.C., Hamburger, D.S., Riggins, R.B., Fernandez, D.R., Zwart, A., Wang, A. & Clarke, R. "Tumor suppressor activities of interferon regulatory factor-1 in human breast cancer associated with caspase activation and induction of apoptosis." Carcinogenesis, in press.

Abstracts

- Clarke, R., Riggins, R.B., Bouker, K.B., Nehra, R., Gomez, B. & Zwart, A. "Molecular mechanisms of endocrine resistance in breast cancer." Anticancer Res, 24: 3455-3456, 2004.

- Wang, Y., Xuan, J., Lee, R.Y., Zhu, Y. & Clarke, R. "In silico correcting for tissue heterogeneity in gene expression profiling of tumors." Anticancer Res, 24: 3456, 2004.

*We include in the appendix reprints of those papers that are already published. Manuscripts cited as "in press" will be included in the next annual report, once reprints are available. We do not include the abstracts, but can do so if requested by either the reviewers and/or DOD. Several other manuscripts related to our bioinformatic methods also are submitted and in preparation; these will be included as appropriate in later annual reports

CONCLUSIONS

We have made good progress on the research infrastructure goals and in the development or optimization of the methods needed for data analysis. We also have completed and published most of the data presented as preliminary data in the initial application. The clinical studies were held up by an unexpectedly long delay in obtaining final approval for our existing protocols but this is now taken care of and we are poised to begin analysis of our first series of breast cancer specimens. We are confident that we can maintain a high level of productivity and remain on target to complete the studies by the end of the funding period.

REFERENCES

1. Early Breast Cancer Trialists' Collaborative Group. Tamoxifen for early breast cancer: an overview of the randomized trials. Lancet, *351*: 1451-1467, 1998.

2. Early Breast Cancer Trialists Collaborative Group: Systemic treatment of early breast cancer by hormonal, cytotoxic, or immune therapy. Lancet, *399*: 1-15, 1992.

3. Winer, E. P., Hudis, C., Burstein, H. J., Chlebowski, R. T., Ingle, J. N., Edge, S. B., Mamounas, E. P., Gralow, J., Goldstein, L. J., Pritchard, K. I., Braun, S., Cobleigh, M. A., Langer, A. S., Perotti, J., Powles, T. J., Whelan, T. J., and Browman, G. P. American Society of Clinical Oncology technology assessment on the use of aromatase inhibitors as adjuvant therapy for women with hormone receptor-positive breast cancer: status report 2002. J Clin Oncol, *20*: 3317-3327, 2002.

4. Ravdin, P. Aromatase inhibitors for the endocrine adjuvant treatment of breast cancer. Lancet, *359*: 2126-2127, 2002.

5. Bonneterre, J., Buzdar, A., Nabholtz, J. M., Robertson, J. F., Thurlimann, B., von Euler, M., Sahmoud, T., Webster, A., and Steinberg, M. Anastrozole is superior to tamoxifen as first-line therapy in hormone receptor positive advanced breast carcinoma. Cancer, *92*: 2247-2258, 2001.

6. Baum, M., Buzdar, A. U., Cuzick, J., Forbes, J., Houghton, J. H., Klijn, J. G., Sahmoud, T., and ATAC Trialists Group Anastrozole alone or in combination with tamoxifen versus tamoxifen alone for adjuvant treatment of postmenopausal women with early breast cancer: first results of the ATAC randomised trial. Lancet, *359*: 2131-2139, 2002.

7. Ellis, M. J., Coop, A., Singh, B., Mauriac, L., Llombert-Cussac, A., Janicke, F., Miller, W. R., Evans, D. B., Dugan, M., Brady, C., Quebe-Fehling, E., and Borgs, M. Letrozole is more effective neoadjuvant endocrine therapy than tamoxifen for ErbB-1- and/or ErbB-2-positive, estrogen receptor- positive primary breast cancer: evidence from a phase III randomized trial. J Clin Oncol, *19*: 3808-3816, 2001.

8. Miller, W. R., Anderson, T. J., and Dixon, J. M. Anti-tumor effects of letrozole. Cancer Invest, *20 Suppl 2*: 15-21, 2002.

9. Smith, I. E. and Dowsett, M. Aromatase inhibitors in breast cancer. N Engl J Med, *348*: 2431-2442, 2003.

10. Clarke, R., Leonessa, F., Welch, J. N., and Skaar, T. C. Cellular and molecular pharmacology of antiestrogen action and resistance. Pharmacol Rev, *53*: 25-71, 2001.

11. Clarke, R. and Brünner, N. Acquired estrogen independence and antiestrogen resistance in breast cancer: estrogen receptor-driven phenotypes? Trends Endocrinol Metab, *7*: 25-35, 1996.

12. Clarke, R., Skaar, T. C., Bouker, K. B., Davis, N., Lee, Y. R., Welch, J. N., and Leonessa, F. Molecular and pharmacological aspects of antiestrogen resistance. J Steroid Biochem Mol Biol, *76*: 71-84, 2001.

APPENDICES

Three reprints are included as appendix materials.

1. Wang, Y., Wang, Z., Xuan, J., Zhang, J., Hoffman, E.P., Clarke, R. & Khan, J. "Optimizing multilayer perceptrons by discriminatory component analysis." Proc IEEE Workshops Machine Learn Signal Process, Sao Luis, Brazil, pp. 273-282, 2004.

2. Bouker, K.B., Skaar, T.C., Fernandez, D.R., O'Brien, K.A., Riggins, R.B., Honghua, C. & Clarke, R. "Interferon regulatory factor-1 mediates the proapoptotic but not cell cycle arrest effects of the steroidal antiestrogen ICI 182,780 (Faslodex, Fulvestrant)." Cancer Res, 64:4030-4039, 2004.

3. Riggins, R.B., Nehra, R., Zwart, A., Agarwal, P. & Clarke, R. "The NFκB inhibitor parthenolide restores ICI 182,780 (Faslodex; Fulvestrant)-induced apoptosis in antiestrogen resistant breast cancer cells." Mol Cancer Ther, 4: 323-412, 2005.

2004 IEEE Workshop on Machine Learning for Signal Processing

OPTIMIZING MULTILAYER PERCEPTRONS BY DISCRIMINATORY COMPONENT ANALYSIS

Yue Wang, Zuyi Wang, Jianhua Xuan, Junying Zhang,
Eric P. Hoffman, Robert Clarke, and Javed Khan
Department of Electrical and Computer Engineering, Virginia Polytechnic Institute and State University, Alexandria, VA 22314 USA
Department of Electrical Engineering and Computer Science, The Catholic University of America, Washington, DC 20064 USA
Research Center for Genetic Medicine, Children's National Medical Center, Washington, DC 20010, USA
Departments of Oncology, Physiology & Biophysics, Georgetown University, Washington, DC 20007, USA
Pediatric Oncology Branch, Advanced Technology Center, National Cancer Institute, Gaithersburg, Maryland 20850, USA

Abstract. Multilayer perceptrons offer an integrated procedure for feature extraction and Bayes classification by learning the decision boundary. Its feed-forward autoassociative architecture can also be used to construct subspaces in a supervised or unsupervised model [1]. On the other hand, multiclass linear discriminant analysis provides a multivariate prediction by estimating the density function. Its linear subspaces obtained by the weighted Fisher criteria under a standard finite normal mixture model retain most closely the intrinsic Bayes separability [2]. Here we show a twofold connection between multilayer perceptrons and linear discriminant analysis using discriminatory component analysis. This theoretical observation immediately suggests a possible clustering-model supported optimization mechanism for multilayer perceptrons: the weights between the input and hidden layers are related to eigenvectors of the weighted Fisher scatter matrix, the number of the hidden layer neurons is justified by the corresponding significant eigenvalues, and the weights connected to the output neurons are obtained from the centers of the classes in the extracted feature subspaces.

INTRODUCTION

Multilayer perceptrons (MLP) offer an integrated procedure for feature extraction and Bayes classification by learning the decision boundary. Its feed-forward autoassociative architecture can also be used to construct nonlinear subspaces in a supervised or unsupervised model [1,3]. The output of each hidden layer may be interpreted as a set of new features presented to the output layer for classification [1]. Such feature extraction actually has various functions. For example, one typical utility is to perform dimensionality reduction [1]. Another popular application is to transform a nonlinearly separable problem into a linear

0-7803-8608-6/04/$20.00 ©2004 IEEE

classification [3]. When both functions are required, multiple hidden layers may be needed [1,3].

On the other hand, multiclass linear discriminant analysis provides a multivariate prediction by estimating the density function. Its subspaces obtained by the weighted Fisher criteria (wFC) under a standard finite normal mixture (SFNM) model retain most closely the intrinsic Bayes separability [2]. It can be shown that the determination of the linear dimension reduction (LDR) transform is equivalent to finding the maximum-likelihood parameter estimates of a SFNM model [2,4]. This motivates an exploration of the connections between MLP and LDR. A natural hypothesis is that the class labels are used as targets during supervised training, forcing the outputs of the hidden layer to capture the most discriminatory components or subspaces, so as to maximize the classification performance of the output layer [1]. Furthermore, the output neuron in MLP plays a similar role as the perceptron. It bears a close resemblance to Fisher's linear discriminant analysis (LDA) [3], and has been generalized to multiple classes [2,5].

Based on these theoretical observations, we therefore wish to suggest an optimization mechanism for multilayer perceptrons. The issues at hand include initialization of the weights between input, hidden, and output layers; and the determination of the numbers of hidden and output neurons. We demonstrate the principle of the method on both simulated and real-world data sets.

THEORY AND METHOD

When there are more than two classes, the task is intrinsically a nonlinear classification problem. Our initial discussion will focus on multiclass cases where all class-pairs are linearly separable, and we will then propose our strategies to more general nonlinearly separable cases.

Linear Dimension Reduction and Feature Extraction

Consider a given m_0-dimensional input **t**-space, multiclass LDR is to search for a linear transformation **W** that reduces the dimensionality to a lower m_1-dimensional feature **x**-space ($m_1 << m_0$), while preserving a maximum amount of discrimination information. Since it is too complex to use the Bayes error directly as a criterion, the most well-known technique is LDA that determines the projection matrix such that the Fisher criterion of total scatter versus average within-class scatter is maximized [1]. It has been shown that when there are more than two classes ($K_0 > 2$), the Fisher criterion that uses the squared Mahanalobis distance between the classes in the dimension reduced subspace is suboptimal with respect to classification, since large between-class distances are overemphasized and the resulting projection preserves the distances of already well-separated classes, causing a large overlap of neighboring classes [2].

By a decomposition of individual class pairs, the wFC was recently proposed in order to improve upon LDA in which the weighting for the contribution is

derived from an attempt to approximate the Bayes error for pairs of classes, taking a sum of the following general form [2]

$$J_{wFC}(\mathbf{W}) = \sum_{k=1}^{K_0-1} \sum_{l=k+1}^{K_0} \pi_k \pi_l \omega(\Delta_{kl}) \text{trace}\left(\mathbf{W}^T \mathbf{S}_{tw}^{-1} \mathbf{S}_{tkl} \mathbf{W}\right) \quad (1)$$

where π_k and π_l are the prior probabilities of classes k and l, $\mathbf{S}_{tw}=\sum_K \pi_k \mathbf{C}_{tk}$ is the pooled within-class scatter matrix, $\mathbf{S}_{tkl}=(\boldsymbol{\mu}_{tk}-\boldsymbol{\mu}_{tl})(\boldsymbol{\mu}_{tk}-\boldsymbol{\mu}_{tl})^T$ is the between-class scatter matrix, and $\omega(\Delta_{kl})$ is the weighting function that depends on the Mahalanobis distance $\Delta_{kl}=[(\boldsymbol{\mu}_{tk}-\boldsymbol{\mu}_{tl})^T \mathbf{S}_{tw}^{-1} (\boldsymbol{\mu}_{tk}-\boldsymbol{\mu}_{tl})]^{1/2}$ between the classes k and l, with class mean vector $\boldsymbol{\mu}_t$ and covariance matrix $\mathbf{C}_t$. Furthermore, the weighting function that approximates the Bayes error rate between the classes via criterion (1) can be shown to take an expression of the following form [2]

$$\omega(\Delta_{kl}) = \frac{1}{2\Delta_{kl}^2} \text{erf}\left(\frac{\Delta_{kl}}{2\sqrt{2}}\right) \quad (2)$$

where $\Delta_{kl}=\|\boldsymbol{\mu}_{tk}-\boldsymbol{\mu}_{tl}\|$ comes down to the ordinary Euclidean distance between class means, and erf(.) is the standard Gaussian error function [2].

Finding a solution $\mathbf{W}$ that maximizes such a criterion (1) comes down to determining an eigenvalue decomposition of the matrix

$$\mathbf{S}_{tw}^{-1} \sum_{k=1}^{K_0-1} \sum_{l=k+1}^{K_0} \pi_k \pi_l \omega(\Delta_{kl}) \mathbf{S}_{tkl} \quad (3)$$

and constructing $\mathbf{W}$ by taking the m_1 eigenvectors corresponding to the m_1 largest eigenvalues [1], namely discriminatory component analysis (DCA). Although both $\mathbf{S}_{tw}^{-1}$ and $\mathbf{S}_{tkl}$ are symmetric, however, matrix (3) is generally not symmetric, resulting in possibly complex-valued eigenvalues and eigenvectors. An elegant yet simple alternative is to determine an eigenvalue decomposition of the generalized between-class scatter matrix

$$\sum_{k=1}^{K_0-1} \sum_{l=k+1}^{K_0} \pi_k \pi_l \omega(\Delta_{kl}) \mathbf{S}_{tw}^{-1/2} \mathbf{S}_{tkl} \mathbf{S}_{tw}^{-1/2} \quad (4)$$

and constructing the interim LDR matrix $\mathbf{W}'$ similarly as aforementioned. Notice that matrix (4) is always symmetric. It can be shown that $\mathbf{W}=\mathbf{W}'\mathbf{S}_{tw}^{-1/2}$ maximizes the original criterion (1).

Having determined LDR matrix $\mathbf{W}$, the dimension reduced feature subspaces become $\mathbf{x}=\mathbf{W}^T(\mathbf{t}-\mathbf{b}_{t0})$, where $\mathbf{b}_{t0}$ is the global center of the data set, and $x_j=\mathbf{w}_j^T(\mathbf{t}-\mathbf{b}_{t0})$ for $j=1, \ldots, m_1$. On the other hand, the output of the hidden layer in MLP is computed as $x_j=\varphi(\mathbf{w}_j^T\mathbf{t}-b_j)$ where $\varphi(.)$ is, often nonlinear, the activation function. The similarity between LDR and feature extraction immediately suggests that the

column vectors of the LDR matrix **W** can be used to initialize the weights between the input and hidden layer of an MLP with a bias $b_j=\mathbf{w}_j^T\mathbf{b}_{t0}$, except for a nonlinear scaling of each new feature. Accordingly, the number of the hidden neurons m_1 shall be justified by the number of the significant eigenvalues of matrix (4). It has been theoretically shown that minimization of the Bayes error with respect to the synaptic weights of the MLP is equivalent to maximizing the criterion (1) that is determined entirely by the hidden neurons of the MLP [3].

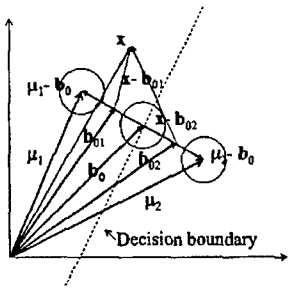

Figure 1. Decision making by a perceptron of 2-output neurons.

Linear Discriminant Analysis and Multiclass perceptrons

As primarily a two-class classifier, LDA describes a linear transformation from an m_1–dimensional problem to a one-dimensional problem [3]. Consider a variable $y=\mathbf{w}^T\mathbf{x}-b$, the LDA is defined by

$$J(\mathbf{w})=\frac{\mathbf{w}^T\mathbf{S}_{xb}\mathbf{w}}{\mathbf{w}^T\mathbf{S}_{xw}\mathbf{w}} \tag{5}$$

that is known as the *generalized Rayleigh quotient*. The solution that maximizes $J(\mathbf{w})$ is simply $\mathbf{w}=\mathbf{S}_{xw}^{-1}(\boldsymbol{\mu}_{xk}-\boldsymbol{\mu}_{xl})$ which is also a generalized eigenvalue problem and referred to as *Fisher's linear discriminant* [3].

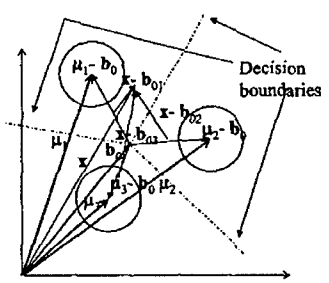

Figure 2. Decision making by perceptron of 3-output neurons.

As aforementioned, the output neuron in the MLP functions similarly as the perceptron that bears a close resemblance to the Bayes classifier, and has been generalized to multiple classes [3]. Specifically, the output neuron in the MLP is computed as $y_i=\varphi(\mathbf{w}_i^T\mathbf{x}-b_i)$, for $i=1, \ldots, m_2$. Consider a two-class case with a linear activation function, we have $y=\mathbf{w}^T\mathbf{x}-b$ with $\mathbf{w}=\mathbf{S}_{xw}^{-1}(\boldsymbol{\mu}_{xk}-\boldsymbol{\mu}_{xl})$ and $b=\mathbf{w}^T\mathbf{b}_{x0}$ where $\mathbf{b}_{x0}=0.5(\boldsymbol{\mu}_{xk}+\boldsymbol{\mu}_{xl})$. We can also use two output neurons to derive a class-dependent representation. Rearrange the output by

$$y=\mathbf{w}^T\mathbf{x}-b=\mathbf{w}_k^T\mathbf{x}-b_k-\left(\mathbf{w}_l^T\mathbf{x}-b_l\right)=y_k-y_l \tag{6}$$

where $\mathbf{w}_k=\mathbf{S}_{xw}^{-1}(\boldsymbol{\mu}_{xk}-\mathbf{b}_{x0})$, $\mathbf{w}_l=\mathbf{S}_{xw}^{-1}(\boldsymbol{\mu}_{xl}-\mathbf{b}_{x0})$, $b_k=\mathbf{w}_k^T\mathbf{b}_{x0}$, and $b_l=\mathbf{w}_l^T\mathbf{b}_{x0}$, we have $y_k=\mathbf{w}_k^T\mathbf{x}-b_k$ and $y_l=\mathbf{w}_l^T\mathbf{x}-b_l$. Fig. 1 illustrates such an interpretation.

Once again, the class-dependent Fisher's linear discriminant $\mathbf{w}_i$ and related bias b_i derived above can be used to initialize the weights between the hidden and output neurons for $i=1, \ldots, m_2$, except for a nonlinear scaling of each output. For example, for a three-class problem, it would be straightforward to have $\mathbf{w}_1=\mathbf{S}_{xw}^{-1}(\boldsymbol{\mu}_{x1}-\mathbf{b}_{x0})$, $\mathbf{w}_2=\mathbf{S}_{xw}^{-1}(\boldsymbol{\mu}_{x2}-\mathbf{b}_{x0})$, $\mathbf{w}_3=\mathbf{S}_{xw}^{-1}(\boldsymbol{\mu}_{x3}-\mathbf{b}_{x0})$, $b_1=\mathbf{w}_1^T\mathbf{b}_{x0}$, $b_2=\mathbf{w}_2^T\mathbf{b}_{x0}$, and $b_3=\mathbf{w}_3^T\mathbf{b}_{x0}$. Fig. 2 illustrates such a case. Notice that such an initialization is readily applicable to single layer perceptrons.

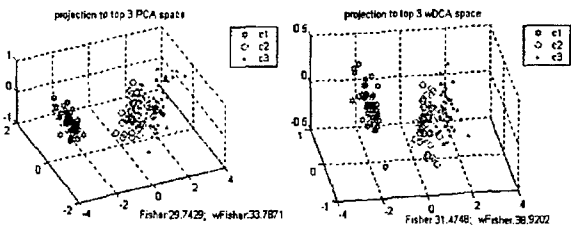

Figure 3. Class separability visualized in the top 3 PCA and wFC-DCA spaces.

EXPERIMENTAL VALIDATION

So far, we have described the theoretical observations on the connections between MLP and wFC-DCA, and have presented the hypotheses of utilizing wFC-DCA to optimize MLP. We shall now illustrate the effectiveness of the proposed methods.

The first experiment reports the test on the Iris data set (m_2=3 classes, 50 samples per class, m_0=4 dimensions). We compared the class separability by wFC-DCA to that by the popular principle component analysis (PCA) [5]. The improvement was obtained by 15%. Fig. 3 illustrates the class separability in three-dimensional plot. We further used wFC-DCA to initialize the MLP and compare the classification results with that of the randomly initialized MLP. In average across m_1=2,3,4, the classification accuracy increases from 62% to 66%.

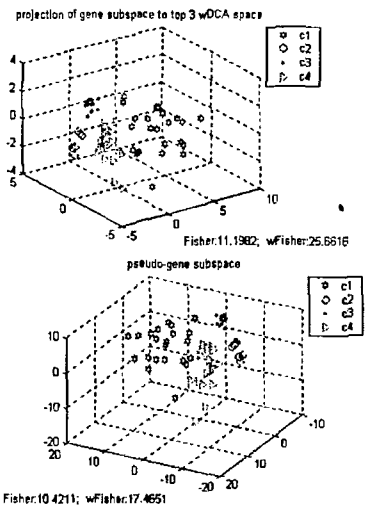

Figure 4. Data plots in the top wFC-DCA and MLP extracted pseudo-gene spaces.

We then tested wFC-DCA-MLP method on a publicly available SRBCT microarray gene expression data set consisting of m_2= 4 different small round blue cell tumors [5]. From total 2308 expressed genes, we selected m_0=5~8 genes for the further study. We first used single layer perceptrons with wFC-DCA extracted pseudo-genes as inputs and compared the classification performance to that of using PCA as previously reported [5]. The results show that, using only top 3~5 such pseudo-genes, 100% prediction accuracy on the total 64 samples estimated by a 3-fold cross-validation can be achieved. We further tested a wFC-DCA optimized MLP and compared the classification performance with that of the randomly initialized MLP on the same data set. The results consistently show that, using only 3 top pseudo-genes, i.e., 3 hidden neurons, the classification accuracy has been increased from 85% to 100% on the total 64 samples estimated by a 3-fold cross-validation. Fig. 4 shows the close yet improved patterns of data plots in the pseudo-genes spaces that were initialized by wFC-DCA and refined by the synaptic weights learning in the MLP. As expected, we have also found that these 3 dominant pseudo-genes contained more than 80% of the total intrinsic Bayes class separability [2].

	Misclassification rate (mean)	Misclassification rate (standard deviation)	Mean squared error during training
MLP with wFC-DCA initialization	0.47%	0.0141	0.0169
MLP with random initialization	1.4%	0.0656	0.0279

Table 1. Classification performance of the MLP with wFC-DCA and random initializations on the simulated data set.

	Misclassification rate (mean)	Misclassification rate (standard deviation)	Mean squared error during training
MLP with wFC-DCA initialization	5.23%	0.0635	0.0032
MLP with random initialization	11.2%	0.1672	0.0755

Table 2. Classification performance of the MLP with wFC-DCA and random initializations on the SRBCT data set.

To obtain more quantitatively comparisons, we applied our method to a simulated data set with m_0=4 and m_2= 3. The performance was estimated via a 3-fold cross-validation. We compared the performance of the MLP with random and wFC-DCA initializations in terms of the averaged misclassification rate and its standard deviation, with 200 trials for each case. Table 1 reports the validation results. These controlled experiments shown that with wFC-DCA initialization, MLP reached faster and more global convergence in that it used much less epochs and reached higher and more robust prediction accuracy.

As an example of more challenging problems and more rigorous efforts, we conducted additional validations on the SRBCT data set now with m_0=20 top discriminatory genes to assess the impact of the proposed optimization on easing the curse of dimensionality. Once again, the performance was estimated via a 3-fold cross-validation, and we compared the performance of the MLP with random and wFC-DCA initializations in terms of the averaged misclassification rate and its standard deviation, with 200 trials for each case. Table 2 reports the validation results. From Fig. 5, it can be seen that when the MLP is initialized by the wFC-DCA that has an initial lower mean squared error (MSE) of 0.00000388, the refined pseudo-genes via the converged weights of the MLP were very close to the wFC-DCA extracted ones. Not surprisingly, when the MLP is initialized randomly with a high initial MSE of 0.1279, the converged weights of the MLP were trapped into the local optimum and deviated from the correct ones. Notice that the correctly extracted discriminatory pseudo-genes shall support a higher separability between the classes.

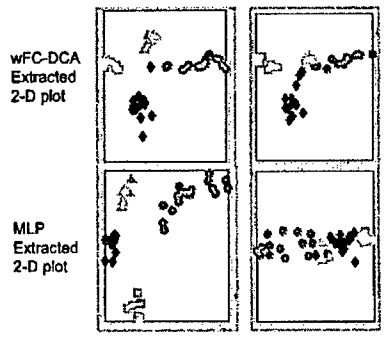

Figure 5. SRBCT plots in the top wFC-DCA and MLP extracted pseudo-gene spaces (left: by wFC-DCA initialization. Right: by random initialization).

As a final test, we considered the ALL-AML dataset of the acute leukemias where m_0=20 and m_2=4. Since the sample size is relatively small, we used a 5-fold cross validation to estimate the classification performance. Once again, we compared the performance of the MLP with random and wFC-DCA initializations in terms of the averaged misclassification rate and its standard deviation, with 200 trials for each case. Table 3 reports the validation results and Fig. 6 provides the further evidence of the positive impact of the wFC-DCA initialization on the performance of the MLP.

	Misclassification rate (mean)	Misclassification rate (standard deviation)	Mean squared error during training
MLP with wFC-DCA initialization	3.57%	0.0301	0.0684
MLP with random initialization	22.6%	0.2446	0.4862

Table 3. Classification performance of the MLP with wFC-DCA and random initializations on the ALL-AML data set.

Thus, we see that wFC-DCA based MLP optimization works reasonably well as expected. When the distributions of the data set are close to SFNM that can be

effectively visualized and estimated using our VIsual and Statistical Data Analyzer (VISDA) software (http://www.cbil.ece.vt.edu/software) [4], it gives excellent results. When the distributions of the data set are multimodal in nature with non-Gaussian classes, the optimization is less effective but still quite reasonable. However, if the classes are highly nonlinear separable, more care shall be taken to fully utilize the proposed method. While the effectiveness of this method may be data-dependent, we would expect it to be a very useful tool in the design of the MLP classifiers, given the unavailability of the general case-specific guidelines [6].

DISCUSSIONS

We have shown a close connection between classification by MLP and classification by LDA. By suggesting a wFC-DCA based optimization procedure for improving the utility of MLP, our main contribution lies in the theoretical insight and experimental validation on what MLP is doing.

One important consideration with the present MLP optimization is that the complexity of the MLP (e.g., total number of the freely adjustable synaptic weights in the network) should be minimized in order to ease the curse of dimensionality [1]. From our later experimental results, it can be seen that the estimated generalizable performance, as expected, decreased with the increase in the input dimensions (e.g., m_0=20 versus m_0=5~8).

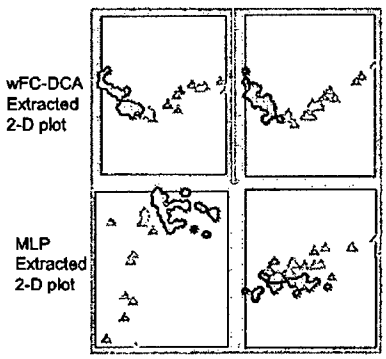

Figure 6. ALL-AML plots in the top wFC-DCA and MLP extracted pseudo-gene spaces (left: by wFC-DCA initialization. Right: by random initialization).

It must be noted, however, that LDR/LDA belongs to probability density based method that assumes Gaussian model for each class by model estimation, while MLP belongs to geometric approach that finds the decision boundary directly from maximizing classification accuracy. From Vapnik's philosophy of learning theory [1,3], the further trained MLP often outperforms the initial wFC-LDA. Our experimental results also support such an expectation, particularly when the data distributions deviate from SFNM or the sample size is simply too small.

Although wFC-DCA is successful in optimizing the MLP in multiclass classification, this success does not imply that the method can be effective for any data set, such as multiclass nonlinearly separable cases. A classification problem could be an intrinsically nonlinear problem, or becomes a nonlinear problem after dimensionality reduction according to Cover's theorem on the separability of

patterns [3]. As aforementioned, therefore, the hidden layer of the MLP needs to perform the additional function of transforming a nonlinearly separable problem into a linear classification. This may be achieved by the existing hidden layer through dual-purpose training, or one additional hidden layer shall be introduced [3]. An elegant yet simple method is to apply divide-and-conquer principle to the data set and accordingly introduce some pseudo-classes to the output layer, such that all class-pairs are linearly separable thereafter. Notice that the discrete decision fusion can be readily and effortlessly done without using any combiner, since the pseudo-classes belong to some of the known classes as a priori. It shall not escape our notice that a net reduction in MLP complexity can still be achieved when m_0 is large, since the total number of weights in a three-layer MLP is $m_1(m_0+m_2)$ such that the reduction due to m_1 surpasses the generally limited increase due to m_2. Further refinements include methods that allow a co-determination of m_1 and m_2 for an optimum generalizable performance when the curse of dimensionality is the issue [1,3,4,5,7].

Appendix

Computation of $\mathbf{S}_{tw}^{-1/2}$:

Let the eigenvalue decomposition of $\mathbf{S}_{tw}$ be $\mathbf{S}_{tw}=\mathbf{EDE}^T$ where $\mathbf{E}$ is the orthogonal matrix of eigenvectors of $\mathbf{S}_{tw}$ and $\mathbf{D}$ is the diagonal matrix of its eigenvalues, then $\mathbf{S}_{tw}^{-1/2}=\mathbf{ED}^{-1/2}\mathbf{E}^T$ where the matrix $\mathbf{D}^{-1/2}$ is computed by a simple componentwise operation [8].

Acknowledgement

This work was supported in part by the National Institutes of Health under Grants CA83231, CA109872, CA096483, CA100970, and NS029525.

REFERENCES

[1] A. K. Jain, R. P. W. Duin, and J. Mao, "Statistical pattern recognition: a review," *IEEE Trans. Pattern Anal. Machine Intell.*, vol. 22, no. 1, pp. 4-37, Jan. 2000.

[2] M. Loog, R. P. W. Duin, and R. Haeb-Umbach, "Multiclass linear dimension reduction by weighted pairwise Fisher criteria," *IEEE Trans. Pattern Anal. Machine Intell.*, vol. 23, no. 7, pp. 762-766, July 2001.

[3] S. Haykin, *Neural Networks: A Comprehensive Foundation*, 2nd ed., New Jersey: Prentice-Hall, 1999.

[4] Y. Wang, L. Luo, M. T. Freedman, and S-Y Kung, "Probabilistic principal component subspaces: A hierarchical finite mixture model for data visualization," *IEEE Trans. Neural Networks*, vol. 11, no. 3, pp. 625-636, May 2000.

[5] J. Khan, et al., "Classification and diagnostic prediction of cancers using gene expression profiling and artificial neural networks," *Nature Medicine*, vol. 7, no. 6, pp. 673-679, June 2001.
[6] A. Hyvarinen and E. Bingham, "Connection between multilayer perceptrons and regression using independent component analysis," *Neurocomputing*, vol. 50, pp. 211-222, 2003.
[7] K. Z. Mao, "RBF neural network center selection based on Fisher ratio class separability measure," *IEEE Trans. Neural Networks*, vol. 13, no. 5, pp. 1211-1217, Sept. 2002.
[8] A. Hyvarinen, J. Karhunen, and E. Oja, *Independent Component Analysis*, New York: John Wiley, 2001.

[CANCER RESEARCH 64, 4030–4039, June 1, 2004]

Interferon Regulatory Factor-1 Mediates the Proapoptotic but Not Cell Cycle Arrest Effects of the Steroidal Antiestrogen ICI 182,780 (Faslodex, Fulvestrant)

Kerrie B. Bouker,[1] Todd C. Skaar,[1,3] David R. Fernandez,[1] Kerry A. O'Brien,[1] Rebecca B. Riggins,[1] Donghua Cao,[4] and Robert Clarke[1,2]

[1]Department of Oncology and Lombardi Comprehensive Cancer Center and [2]Department of Physiology and Biophysics, Georgetown University School of Medicine, Washington, District of Columbia, and [3]Division of Clinical Pharmacology and [4]Department of Pharmacology and Toxicology, Indiana University Cancer Center and Department of Medicine, Indianapolis, Indiana

ABSTRACT

Antiestrogens induce both cytostasis (cell cycle arrest) and apoptosis, but the relationship between these end points and the signaling that regulates their induction are unclear. We have previously implicated the transcription factor and putative tumor suppressor IFN regulatory factor-1 (IRF-1) in acquired antiestrogen resistance (Gu *et al.*, Cancer Res, *62:* 3428–3437, 2002). We now show the functional significance of IRF-1 in affecting antiestrogen responsiveness in estrogen receptor-positive antiestrogen-sensitive models (MCF-7, T47D, and ZR-75-1), a model of acquired antiestrogen resistance (MCF7/LCC9; estrogen receptor positive), and a model of *de novo* antiestrogen resistance (MDA-MB-231; estrogen receptor negative). Basal IRF-1 mRNA expression is lower in MCF7/LCC9 cells when compared with MCF-7, T47D, and ZR-75-1 cells. IRF-1 transcriptional activity in MCF-7/LCC9 cells is 18-fold lower than that seen in the parental cells (MCF-7/LCC1) and is comparable with that in MDA-MB-231 cells. Although IRF-1 mRNA expression is induced by ICI 182,780 in sensitive cells, this regulation is lost in MCF-7/LCC9 and is absent in MDA-MB-231 cells. Loss of IRF-1 regulation appears specific to antiestrogen resistance—resistant cells induce IRF-1 mRNA in response to the cytotoxic drug doxorubicin. A dominant-negative IRF-1 eliminates the ICI 182,780-induced apoptotic response (reduced >4-fold) and reduces MCF-7 and T47D cell sensitivity to the antiproliferative effects of ICI 182,780. This effect is not mediated by changes in cell cycle distribution; rather, dominant-negative IRF-1 reduces ICI 182,780-induced apoptosis. These data identify a novel mechanism of antiestrogen resistance and implicate IRF-1 as a key component in signaling some ER-mediated effects on apoptosis/cell survival.

INTRODUCTION

For many women, antiestrogen therapy is the least toxic and most effective means to manage their hormone-dependent breast cancer. The most widely studied antiestrogen has been tamoxifen (TAM), which can increase both disease-free and overall survival in breast cancer patients, reduce the incidence of estrogen receptor-positive (ER+) disease in high-risk women, and reduce the rate of bone loss from osteoporosis (1, 2). Although first line antiestrogen therapy remains the standard of care for these patients (3–5), approximately one-third of all ER+ breast tumors exhibit *de novo* antiestrogen resistance, and most initially responsive tumors eventually acquire resistance (6).

The steroidal antiestrogen ICI 182,780 (Faslodex; Fulvestrant) has successfully completed clinical trials and exhibits considerable potential for more widespread clinical use (7). Most currently available antiestrogens show little or no significant activity in TAM-resistant disease, which is often treated with a second-line aromatase inhibitor. However, ICI 182,780 is clearly active in patients who have received TAM treatment and eventually recurred (8). Furthermore, two Phase III clinical trials in TAM-resistant patients have shown ICI 182,780 to be at least as effective as the potent aromatase inhibitor anastrazole (9, 10). Unlike most other antiestrogens, ICI 182,780 is a pure ER antagonist (11) that can induce degradation of ER protein (12) and inhibit receptor dimerization (13). Furthermore, ICI 182,780 is devoid of the uterotropic activity associated with the ability of TAM to increase the risk of developing endometrial cancers (8, 14).

Antiestrogen and estrogen responsiveness are complex phenotypes, and both genomic and nongenomic activities are functionally implicated (6, 15). In sensitive cells, antiestrogens are clearly cytostatic, inducing a G_0-G_1 cell cycle arrest *in vitro*. Clinically, the ability of antiestrogens to induce significant reductions in tumor size and increases in overall survival (1, 2) and to inhibit the development of ER+ tumors in the chemopreventive setting (16, 17) strongly suggest that these drugs also may be cytotoxic. Evidence implicates an induction of apoptotic cell death as the major mechanism through which antiestrogens might induce a cytotoxic effect (6). However, the relationship between growth arrest and apoptosis and how antiestrogens functionally affect cell signaling to regulate these two end points remains to be firmly established.

It is becoming apparent that antiestrogen resistance in ER+ tumors is unlikely to be driven by a single gene/signaling pathway. Thus, we have invoked a gene network hypothesis that confers diversity in estrogen/antiestrogen-initiated signaling (15, 18, 19). Ultimately, we envision multiple concurrent signals through this network of integrated and potentially interdependent pathways, some antiapoptotic and some proapoptotic, with cellular response reflecting the dominant signals. In antiestrogen-unresponsive cells, we hypothesize that the endocrine regulation and/or function of key components of this network is changed and that proapoptotic signals are no longer induced and antiapoptotic signals have become dominant. To begin identifying key genes that may make up such a network, we have applied both serial analysis of gene expression and gene expression microarray analyses to a series of antiestrogen-sensitive and -resistant cells. Among the key genes identified is the putative tumor suppressor gene IFN regulatory factor-1 (IRF-1; Ref. 19).

Although initially identified as an IFN-responsive gene, IRF-1 has shown activity as a tumor suppressor in several studies (20–22). For example, IRF-1 is deleted in some cancers (23, 24), and loss of IRF-1 significantly increases tumorigenicity in mouse models driven either by ras or loss of p53 (25). IRF-1 can signal to apoptosis in a p53-dependent or -independent manner (26, 27); with or without induction of $p21^{waf1/cip1}$ (26) or $p27^{kip1}$ (28); and through caspase-1 (27), caspase-7 (29), caspase-8 (30), and/or Fas ligand (31). Loss of p53 activity is common in breast cancer (32). Nonetheless, many breast cancers are initially responsive to cytotoxic drugs and hormones (1, 33), implying that drug-induced apoptosis likely occurs through both p53-dependent and -independent mechanisms. TAM-

Received 11/17/03; revised 2/26/04; accepted 3/29/04.

Grant support: Public Health Service Award R01-CA/AG58022-10 (R. Clarke), Department of Defense Awards DAMD17-99-9189 (K. Bouker), DAMD17-99-1-9191, BC010619, and BC990358 (R. Clarke) from the United States Army Medical Research and Materiel Command, American Cancer Society Award IRG-97-1520-01-IRG (T. Skaar), and the Charles and Ella O. Latham Charitable Trust (T. Skaar).

The costs of publication of this article were defrayed in part by the payment of page charges. This article must therefore be hereby marked *advertisement* in accordance with 18 U.S.C. Section 1734 solely to indicate this fact.

Requests for reprints: Robert Clarke, Room W405A, Research Building, Department of Oncology, Georgetown University School of Medicine, 3970 Reservoir Road NW, Washington, DC 20007. Phone: (202) 687-3755. Fax: (202) 687-7505. E-mail: clarker@georgetown.edu.

induced growth arrest can occur independently of p53 (34), but the precise signaling responsible for these effects requires additional study. The primary mechanisms of cell growth arrest and apoptosis for ICI 182,780 and the importance of signaling through p53 are unknown.

In addition to our previous study implicating IRF-1 in affecting antiestrogen responsiveness in MCF-7 cells (19), Harroch *et al.* (35) observed that interleukin 6 inhibited proliferation and induced IRF-1 mRNA and IRF-1 binding to its target DNA sequence in T47D cells. In an immunohistochemistry study of IRF-1 expression in breast cancer, the authors report less IRF-1 expression in neoplastic compared with normal human breast, consistent with reduced expression of a putative tumor suppressor gene. However, IRF-1 expression was not assessed in association with established prognostic markers or clinical outcome (36).

In this study, we used the ER− MDA-MB-231 cells as a model of *de novo* antiestrogen resistance (6). To model *de novo* antiestrogen sensitivity, we used the estrogen-dependent, ER+ MCF-7 (37) and T47D cells (38) and the ER+, antiestrogen-sensitive but estrogen-independent MCF-7 variant MCF7/LCC1 (39). As a model of acquired ICI 182,780 resistance, we studied the MCF7/LCC9 cells, which were derived from MCF7/LCC1 cells and are ER+, estrogen independent, and ICI 182,780 and TAM cross-resistant (40). These studies strongly implicate signaling through IRF-1 and its protein partners as a critical mediator of antiestrogen signaling and as a key gene in a broader gene network (15, 19, 41). Hence, we now show that IRF-1 mRNA expression is induced by ICI 182,780 and repressed by estrogens in antiestrogen-sensitive cells. Hormonal regulation of IRF-1 is absent in ER− cells and is specifically lost in ER+ cells with acquired antiestrogen resistance. Both MCF-7 and T47D breast cancer cells expressing a dominant-negative IRF-1 (dnIRF-1) exhibit a decrease in sensitivity to ICI 182,780. The data separate the proapoptotic activity of ICI 182,780 from its ability to induce cell cycle arrest and are consistent with IRF-1 playing a critical role in those proapoptotic activities of antiestrogens most likely to contribute to their ability to increase overall survival and to reduce the risk of developing ER+ breast cancer (1, 16, 42).

MATERIALS AND METHODS

Cell Culture and Reagents. MCF-7, T47D, ZR-75-1 (ER+, estrogen dependent, antiestrogen sensitive), and MDA-MB-231 (ER−, estrogen independent, antiestrogen unresponsive) cells were routinely grown in improved minimal essential medium (IMEM; Biofluids, Rockville, MD) with phenol red and supplemented with 5% fetal bovine serum. MCF-7 cells were originally obtained from Dr. Marvin Rich (Michigan Cancer Foundation, Detroit, MI). T47D, ZR-75-1, and MDA-MB-231 cells were obtained from the Lombardi Comprehensive Cancer Center's Tissue Culture Shared Resource. MCF-7/LCC1 (ER+, estrogen independent, antiestrogen sensitive, MCF-7 variant; Refs. 39 and 43) and MCF-7/LCC9 cells (ER+, estrogen independent, TAM and ICI 182,780 cross-resistant, MCF-7 variant derived directly from MCF7/LCC1 by selection against ICI 182,780; Refs. 19 and 40) were routinely grown in IMEM without phenol red and supplemented with 5% charcoal stripped calf serum-IMEM. All cells were maintained in a humidified incubator at 37°C in an atmosphere containing 95% air:5% CO_2. The steroidal antiestrogen ICI 182,780 (Faslodex; Fulvestrant) was kindly provided by Dr. Alan Wakeling (Zeneca Pharmaceuticals, Macclesfield, Cheshire, United Kingdom). Recombinant human IFN-γ was purchased from Boehringer Mannheim (Mannheim, Germany).

RNA Extraction. Total RNA was extracted from proliferating subconfluent cells using the TRIazol reagent (Life Technologies, Inc., Gaithersburg, MD) according to the manufacturer's instructions. In brief, cells were rinsed with 1× PBS to remove serum and lysed by the addition of the TRIazol reagent. RNA was isolated by chloroform extraction and precipitated using isopropanol. Total RNA was quantified based on the absorbance at 260 nM using a spectrophotometer (DU640; Beckman, Fullerton, CA).

Riboprobe Generation and RNase Protection Analysis. The IRF-1 riboprobe was generated by reverse transcriptase-PCR amplification of a portion of the IRF-1 mRNA from MCF-7 cells. Amplification by PCR applied one 95°C cycle for 3 min, 40 cycles of 95°C for 30 s, 59°C for 30 s, and 72°C for 1 min followed by 1 cycle of 72°C for 5 min, using the following primers: forward, TCCACCTCTCACCAAGAACC (bp 533–552), and reverse, TTCCCTTCCTCATCCTCATC (bp 873–892). To control for equivalent RNA loading, we measured expression of the constitutively expressed 36B4 mRNA that encodes the human acidic ribosomal protein P0 (44). The 36B4 riboprobe was generated as described previously (39).

RNase protection assays were performed as described previously (19, 45). In brief, plasmids were linearized by digestion with *EcoR1* and transcribed with either SP6 (IRF-1) or T7 polymerase (36B4) in the presence of [^{32}P]UTP. To obtain signals of approximately comparable intensity, the 36B4 riboprobes were labeled with approximately one-fifth of the [^{32}P]UTP concentration used to label the IRF-1 riboprobes. The IRF-1 and 36B4 riboprobes respectively generate 360- and 220-bp protected fragments. For each assay, 30 μg of total RNA was hybridized to 5×10^4 dpm of probe for 12–16 h at 50°C and digested with 40 μg/ml RNase A for 30 min at 25°C. Digestion was terminated by the addition of proteinase K (0.25 mg/ml) and 0.5% (w/v) SDS. Samples were extracted into phenol:chloroform:isoamyl alcohol (25:24:1) and precipitated in ethanol, and the pellets were boiled in loading buffer and fractionated in 6% Tris-borate EDTA-urea polyacrylamide gels. Radioactivity was detected by autoradiography and quantified using PhosphorImager analysis (445SI; Molecular Dynamics, Sunnyvale, CA).

Cell Lysis and Immunoblotting. For the determination of IRF-1 protein expression, cells were seeded into 6-well dishes at 2×10^5 cells/well and cultured in normal growth media for 24 h. To examine the induction of IRF-1 in response to ICI 182,780 or estradiol, cells were seeded at 10^5 cells/well 1 day before treatment with either 1 nM 17β-estradiol or 100 nM ICI 182,780 for 3 days. Cells were lysed in modified radioimmune precipitation assay buffer [150 mM NaCl, 50 mM Tris, 1% Igepal CA-630, and 0.5% deoxycholate (pH 7.5)] supplemented with Complete Mini protease inhibitor mixture tablets (Roche, Mannheim, Germany). Lysates were clarified by centrifugation, and equal volumes were added to 2× Laemmli sample buffer before boiling and loading onto precast 12% acrylamide gels (NuPAGE Electrophoresis System, Invitrogen, Carlsbad, CA). Proteins were transferred to nitrocellulose membranes and incubated with primary antibody (IRF-1 C-20 at 1:200; Santa Cruz Biotechnology, Santa Cruz, CA) in Tris Buffered Saline and Tween-20 [TBST; 10 mM Tris HCl, 150 mM NaCl, and 0.05% Tween-20 (pH 8.0)] containing 5% nonfat dry milk overnight at 4°C. Membranes were then incubated with horseradish peroxidase-conjugated secondary antibody for 1 h at room temperature followed by enhanced chemiluminescence (Amersham Biosciences, Piscataway, NJ) and exposure to film (X-OMAT Blue XB-1; Kodak, Rochester, NY). To confirm equal loading, membranes were reprobed as described above using a β-actin monoclonal antibody (1:5000; Sigma, St. Louis, MO).

Generation of dnIRF-1. Although small interfering RNA (siRNA) can be a powerful method to inhibit RNAs, we did not use this method to block IRF-1 because of the recent reports of a marked induction of an IFN response when these molecules are introduced into cells (46, 47). Thus, the best remaining approach was the use of a stably expressed dominant-negative strategy. A wild-type IRF-1 cDNA (kindly provided by Dr. Taniguchi, University of Tokyo, Japan) was subcloned into the *Xho*I site of the pGEM7Z expression vector (Promega, Madison, WI) and linearized with *Bgl*II. The dnIRF-1 comprises the full-length wild-type IRF-1 cDNA with a deletion of bp 647-1173 and contains both the 3′ and 5′ untranslated regions, the DNA-binding domain, and the nuclear localization sequences of IRF-1. We constructed dnIRF-1 by PCR amplification using bp 630–647 (TAGCAGGGCCCCTGG) as the forward primers and bp 1173–1187 (ATCAGAGAAGGTATCAGG) as the reverse primers. PCR conditions were 30 cycles of 95°C for 30 s, 45°C for 45 s, and 72°C for 5 min. Integrity of the dnIRF-1 sequence was confirmed by standard dideoxy-mediated chain-termination sequencing. dnIRF-1 was subcloned into both the *Xho*I site of the pcDNA3 mammalian expression vector (Invitrogen, Carlsbad, CA) and into the *Xho*I site of the pbiEGFP-tet vector [a plasmid expressing enhanced green fluorescent protein (EGFP)] under the control of a bidirectional tetracycline-responsive promoter (Clontech, Palo

Alto, CA). The IRF-1 riboprobe (above) identifies dnIRF-1, generating a 115-bp protected dnIRF-1 fragment.

Transient Transfections and Luciferase Reporter Assay. Cells were transfected using the FuGENE 6 method (Roche Diagnostics, Indianapolis, IN). For reporter assays, 8×10^4 cells/well were plated in 12-well plates and allowed to grow for 24 h before transfection. Cells were cotransfected with the pISRE-luc plasmid (contains five copies of the IFN-stimulated response element; ISRE) as provided in the PathDetect kit (Promega) and with either a standard control comprising a pcDNA3 plasmid without the ISRE or a pcDNA3 plasmid containing the cDNA from either IRF-1 or dnIRF-1. To control for transfection efficiency, a pRL-SV40 plasmid (Promega) containing the *Renilla* luciferase gene under the control of a constitutive SV40 promoter also was cotransfected into cells. One μg of plasmid DNA was added to serum-free media containing the FuGENE 6 reagent and allowed to incubate for 30 min at room temperature. Where appropriate, cells were maintained in growth media with or without 500 IU/ml IFN-γ for 24–48 h. Subsequently, cells were lysed, and activation of the ISRE-luciferase construct was measured using the Dual Luciferase Assay kit (Promega) according to the manufacturer's instructions. Luminescence was quantified using a Lumat LB 9501 luminometer (EG&G Berthold, Bundoora, Victoria, Australia).

Stable Transfection with dnIRF-1. For stable transfections, cells were plated in T-75 cm^2 plastic tissue culture flasks at a density of 0.5×10^6 cells/flask and grown for 24 h before transfection. A total of 8 μg of plasmid DNA were transfected into MCF-7 cells stably transfected with the tetR protein (MCF-7/VP16; generously provided by Dr. Susan Conrad, Michigan State University, East Lansing, MI) or T47D cells using the FuGENE6 method (above). Cells were transfected with either an empty pBI-EGFP-tet plasmid containing the EGFP selectable marker (Clontech) or one containing the dnIRF-1 cDNA and the pBABE plasmid (kindly provided by Dr. Matthew Ellis, Washington University, St. Louis, MO) encoding for puromycin resistance. Stably transfected cells were selected for growth in the presence of 1 μg/ml puromycin. Puromycin-resistant colonies expressing EGFP as measured by standard fluorescence activated cell sorting (FACS) were expanded and screened for expression of the dnIRF-1 by RNase protection. All of the transfectants used in these experiments were from pooled populations. Cells transfected with the empty control vector were designated MCF7/ctrl and T47D/ctrl and those transfected with the dnIRF-1 were designated MCF7/dnIRF-1 and T47D/dnIRF-1.

Cell Proliferation. MCF-7/ctrl, T47D/ctrl, MCF7/dnIRF-1, and T47D/dnIRF-1 cells were sorted aseptically by FACS in the Lombardi Comprehensive Cancer Center Flow Cytometry Shared Resource for EGFP expression and plated into 12-well plastic tissue culture plates at a density of 1.5×10^3 MCF-7 or 2×10^3 T47D cells/well. Twenty-four h post plating, cells were treated with 100 nM or 1 μM ICI 182,780 or vehicle control for 72 h. Cells were then trypsinized, resuspended in PBS, and counted in a Beckman Coulter counter (Beckman Coulter Corp., Fullerton, CA) to assess cellular proliferation.

Cell Cycle Analyses. Cells stably transfected with the dnIRF-1 or empty control plasmids were plated in T-75 cm^2 plastic tissue culture flasks at a concentration of 0.5×10^6 and allowed to grow for 3 days. Cells were then analyzed for alterations in cell cycle via FACS. FACS analysis was conducted by the Lombardi Comprehensive Cancer Center Flow Cytometry Shared Resource, according to the method of Vindelov *et al.* (48).

Apoptosis. Staining for annexin V, an optimal assay for detecting apoptosis in MCF-7 cells (49, 50), was performed according to the manufacturer's instructions (R&D Systems, Minneapolis, MN). Control- or dnIRF-1-transfected MCF-7 cells (1×10^6) were seeded in T-75 cm^2 plastic tissue culture dishes and allowed to grow for 24 h. Cells were then treated with ICI 182,780 or vehicle for 72 h, trypsinized, and pelleted by centrifugation. Cell pellets were rinsed twice in ice-cold PBS and stained with 5 μg/ml 7-aminoactinomycin D for 15 min at room temperature. After staining with 7-aminoactinomycin D, cells were washed and resuspended in annexin V binding buffer [10 mM 4-(2-hydroxyethyl)-1-piperazineethanesulfonic acid/NaOH, 140 mM NaCl, and 2.5 mM $CaCl_2$ (pH 7.4)]. Cells (1×10^5) were then stained with 0.3 μg of phycoerythrin-conjugated annexin V in the dark, and flow cytometric analysis was performed using a FACStar^{Plus} flow cytometer (Becton-Dickinson, Mountain View, CA) to determine the proportion of apoptotic cells in each sample. Apoptosis was measured only in cells expressing the dnIRF-1 transgene or empty vector (as assessed by concurrent EGFP expression).

Statistical Methods. Student's *t* test was used to compare two groups in which the data are normally distributed; a Wilcoxon *t* test was used to compare groups in which data are not normally distributed. For multiple comparisons, ANOVA was used with a *post hoc t* test for multiple comparisons. Where several experimental groups were compared with the same control, we used Dunnett's test (51).

RESULTS

IRF-1 Is Differentially Expressed in Antiestrogen-Sensitive and -Resistant Breast Cancer Cells. We measured basal expression of IRF-1 mRNA by RNase protection analyses in two models of antiestrogen resistance: MCF-7/LCC9 cells (acquired resistance, ER+, ICI 182,780 and TAM cross-resistant) and MDA-MB-231 (*de novo* resistance, ER−, ICI 182,780 and TAM cross-resistant; Ref. 6). MCF-7/LCC9 cells exhibit a 4.2-fold ($P < 0.05$) and 2.6-fold ($P \leq 0.01$) lower expression of IRF-1 mRNA than the antiestrogen-sensitive MCF-7 and MCF-7/LCC1 cells, respectively (Fig. 1, *A* and *B*). IRF-1 mRNA expression in MCF-7/LCC9 cells is not significantly different from that in ER− MDA-MB-231 cells.

The half-life of the IRF-1 protein is less than 30 min, and changes in mRNA levels appear closely associated both with changes in IRF-1 protein expression and IRF-1 transcriptional activity as measured using an ISRE-based promoter-reporter assay (52). To confirm this association, we performed immunoblotting for the cells lines shown in Fig. 1, *A* and *B*. The data in Fig. 1*C* show that, as expected, the mRNA and protein levels are comparable. The MCF-7/LCC1 and MCF-7/LCC9 cells compared here are derived from the same parental MCF-7 cell line and have similar transfection efficiencies as assessed by transfection with β-galactosidase (not shown). Activity of the cotransfected *Renilla* construct (constitutively active) was used to correct for any minor differences in transfection efficiency. MCF-7/LCC9 cells exhibit 18-fold lower basal ISRE activity than their immediate parental cells MCF-7/LCC1 ($P \leq 0.01$; Fig. 1*D*). These data reflect the differential IRF-1 mRNA expression that we have previously detected in gene expression microarrays (19) and now confirm by RNase protection analyses (Fig. 1, *A* and *B*) and immunoblot (Fig. 1*C*). These data also confirm that IRF-1 mRNA expression, protein expression, and transcriptional activation are closely related in breast cancer cells. Furthermore, these data show that IRF-1 expression and activity are significantly lower in ER+ and ER− antiestrogen-resistant cells compared with antiestrogen-sensitive cells.

IRF-1 mRNA Expression Is Regulated through ER in Breast Cancer Cells. Data on basal expression in the sensitive and resistant cells imply that estrogens and antiestrogens may affect IRF-1 mRNA expression. Fig. 2, *A* and *B*, shows the ability of 100 nM ICI 182,780, a clinically relevant concentration (53), to induce IRF-1 mRNA in the three best characterized and most widely used ER+ human breast cancer cell lines (6): MCF-7 ($P \leq 0.001$); T47D ($P \leq 0.001$); and ZR-75-1 ($P < 0.05$). This effect appears to be ER mediated, because IRF-1 mRNA induction by ICI 182,780 is blocked in the presence of estradiol in MCF-7 cells (Fig. 2, *C* and *D*) and ICI 182,780 is unable to induce IRF-1 in the ER− MDA-MB-231 cells (Fig. 2, *A* and *B*).

The dose-response relationships for the endocrine regulation of IRF-1 mRNA in MCF-7 and T47D cells were determined. Cells were plated and 24 h later treated with various doses of ICI 182,780 or 0.1% (v/v) ethanol vehicle for 72–96 h before RNA isolation. ICI 182,780 induces IRF-1 mRNA in a dose-dependent manner, with a maximal 2.5-fold induction at a dose of 100 nM in both MCF-7 (Fig. 3, *A* and *B*; $P \leq 0.001$) and T47D (Fig. 3, *C* and *D*; $P \leq 0.01$) cells. In contrast, IRF-1 mRNA expression is significantly down-regulated in response to treatment with 1 nM estradiol (Fig. 3, *E* and *F*; $P \leq 0.001$).

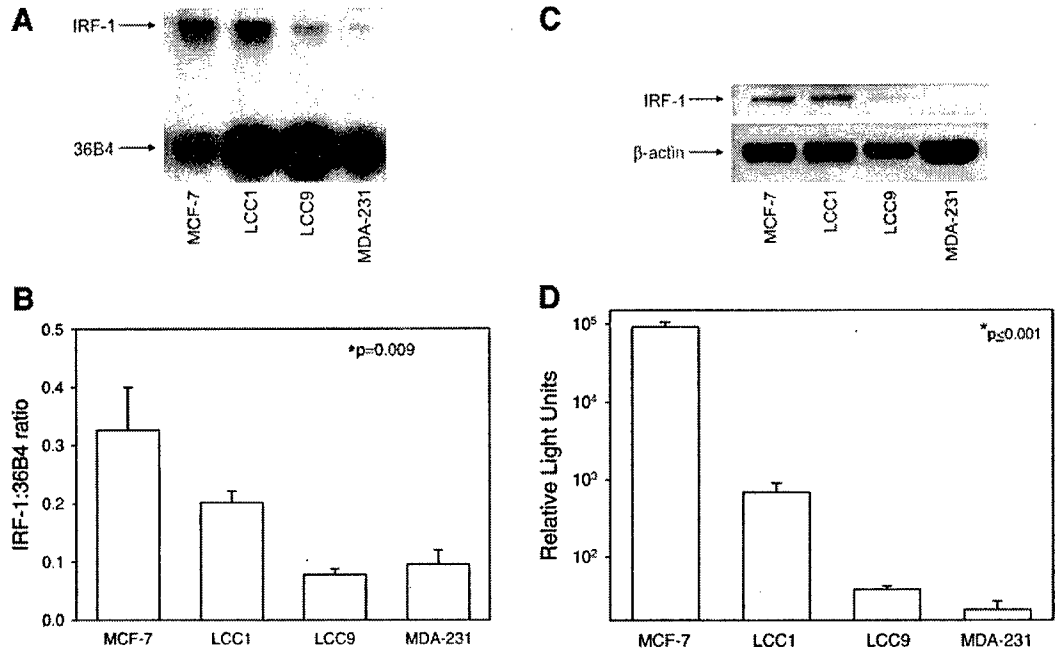

Fig. 1. Basal IRF-1 mRNA and protein expression and transcriptional activation in breast cancer cell lines. *A*, representative RNase protection assay. *36B4*, loading control. *B*, IRF-1 mRNA expression measured by RNase protection and presented as mean ± SE of three determinations, in which intensity is expressed as a ratio of IRF-1:36B4 (ANOVA, $P = 0.009$; *, $P < 0.05$ MCF-7 *versus* MCF7/LCC9; $P < 0.01$ MCF-7/LCC1 *versus* MCF7/LCC9; $P = 0.528$ MDA-MB-231 *versus* MCF7/LCC9). *C*, representative immunoblot of IRF-1 protein. *β-actin*, loading control. *D*, basal transcriptional activity of IRF-1 in breast cancer cell lines (ISRE-luc promoter-reporter assay). Data represent mean ± SE of four determinations and are presented as relative light units. ANOVA, $P < 0.01$; *, $P \leq 0.001$ for MCF-7 *versus* each of MCF7/LCC1, MCF7/LCC9, and MDA-MB-231. *, P = NS for MCF7/LCC9 *versus* MDA-MB-231.

ER-Mediated Regulation of IRF-1 Is Specifically Lost in Anti-estrogen-Resistant Cells. Although the data in Fig. 2 and Fig. 3 show the regulation of IRF-1 mRNA expression, this would likely be of limited functional relevance if similar patterns of regulation occur in antiestrogen-resistant cells. However, the ability of both estrogen and ICI 182,780 to regulate IRF-1 mRNA expression is lost in the MCF-7/LCC9 cells (Fig. 4, *A–D*), and ICI 182,780 is unable to regulate IRF-1 expression in the antiestrogen-resistant ER− cell line, MDA-MB-231 (Fig. 2, *A* and *B*). In contrast, the estrogen-independent but antiestrogen-sensitive MCF7/LCC1 cells retain the ability of estrogen to inhibit IRF-1 mRNA expression (Fig. 4, *A* and *B*). Consistent with the data in Fig. 1, we found similar changes in the hormonal regulation of IRF-1 protein in immunoblots (not shown). MCF7/LCC1 cells do not require estrogens to grow *in vitro* or *in vivo* (estrogen independent) but retain some estrogen responsiveness (40, 43). Thus, the apparent loss of ER-mediated regulation of IRF-1 is associated with acquired antiestrogen resistance but not estrogen independence.

We then asked whether the specificity of endocrine regulation of IRF-1 that is lost in antiestrogen-resistant cells also extended to nonhormonal inducers of IRF-1. In mouse embryonic fibroblasts, IRF-1 is induced by treatment with the cytotoxic drug doxorubicin (26), one of the most active single cytotoxic drugs used in the treatment of breast cancer (54, 55). MCF-7 cells induce IRF-1 mRNA in response to treatment with doxorubicin (Fig. 5, *A* and *B*). Importantly, MCF-7/LCC9 cells retain their ability to regulate IRF-1 expression in response to 1 μM doxorubicin (increase by over 7-fold; $P \leq 0.001$), a response also shared by MDA-MB-231 cells (increase by over 4-fold; $P < 0.05$; Fig. 6, *A* and *B*). Thus, antiestrogen resistance is associated with a specific, ER-mediated change in the regulation of IRF-1 expression, rather than a global loss of IRF-1 mRNA regulation. This specificity allows cells to retain the ability to induce IRF-1 and undergo an IRF-1-regulated apoptotic cell death in response to other cytotoxic agents.

ICI 182,780-Induced Inhibition of Cell Proliferation Is Reduced by dnIRF-1. To study the functional relevance of changes in IRF-1 activity in affecting antiestrogen responsiveness, we created dnIRF-1. dnIRF-1 contains the IRF-1 DNA binding domain and nuclear localization signal but lacks the protein binding and transcriptional activation domains. Dominant-negative activity of dnIRF-1 was apparent in its ability to inhibit basal ISRE activity, activity induced by transient expression of wild-type IRF-1, and IFN-γ stimulated ISRE activity in MCF-7 (Fig. 7; all comparisons $P < 0.001$; Student's *t* test). Control cells transfected with an empty expression vector exhibit no regulation of ISRE activity; control cells transfected with empty luc vector (no ISRE) showed no activity (not shown). Importantly, we did not want dnIRF-1 to eliminate all IRF-1 transcriptional activity but rather to inhibit activity to an extent broadly equivalent to that induced by antiestrogens. Complete loss of IRF-1 could induce compensatory responses of uncertain biological relevance, and there is no evidence that IRF-1 expression is fully lost in breast tumors (36). Because IRF-1 mRNA expression levels are closely related to ISRE activity in breast cells (Fig. 1), the data in Fig. 7 imply that dnIRF-1 inhibits a level of ISRE activity broadly comparable with that induced by antiestrogens in sensitive cells (Fig. 2; Fig. 3).

dnIRF-1 was stably transfected into both MCF-7 and T47D cells, and the ability of dnIRF-1 to affect ICI 182,780-induced inhibition of cell proliferation was measured (Fig. 8, *A* and *B*). In cell proliferation assays, expression of dnIRF-1 significantly reduced responsiveness of the MCF-7/dnIRF-1 and T47D/dnIRF-1 transfectants to ICI 182,780. At 100 nM, the dose that maximally induces IRF-1 mRNA expression, MCF-7/dnIRF-1 and T47D/dnIRF-1 transfectants were significantly less sensitive to ICI 182,780 compared with their respective controls. Similar differences in the responsiveness of MCF-7/dnIRF-1 and T47D/dnIRF-1 cells were seen at 1 μM ICI 182,780 ($P = 0.002$, MCF-7 100 nM ICI 182,780; $P = 0.013$, MCF-7 1 μM ICI 182,780; $P = 0.002$, T47D 100 nM ICI 182,780; $P = 0.043$, T47D 1 μM ICI 182,780; Student's *t* test; Fig. 8, *A* and *B*).

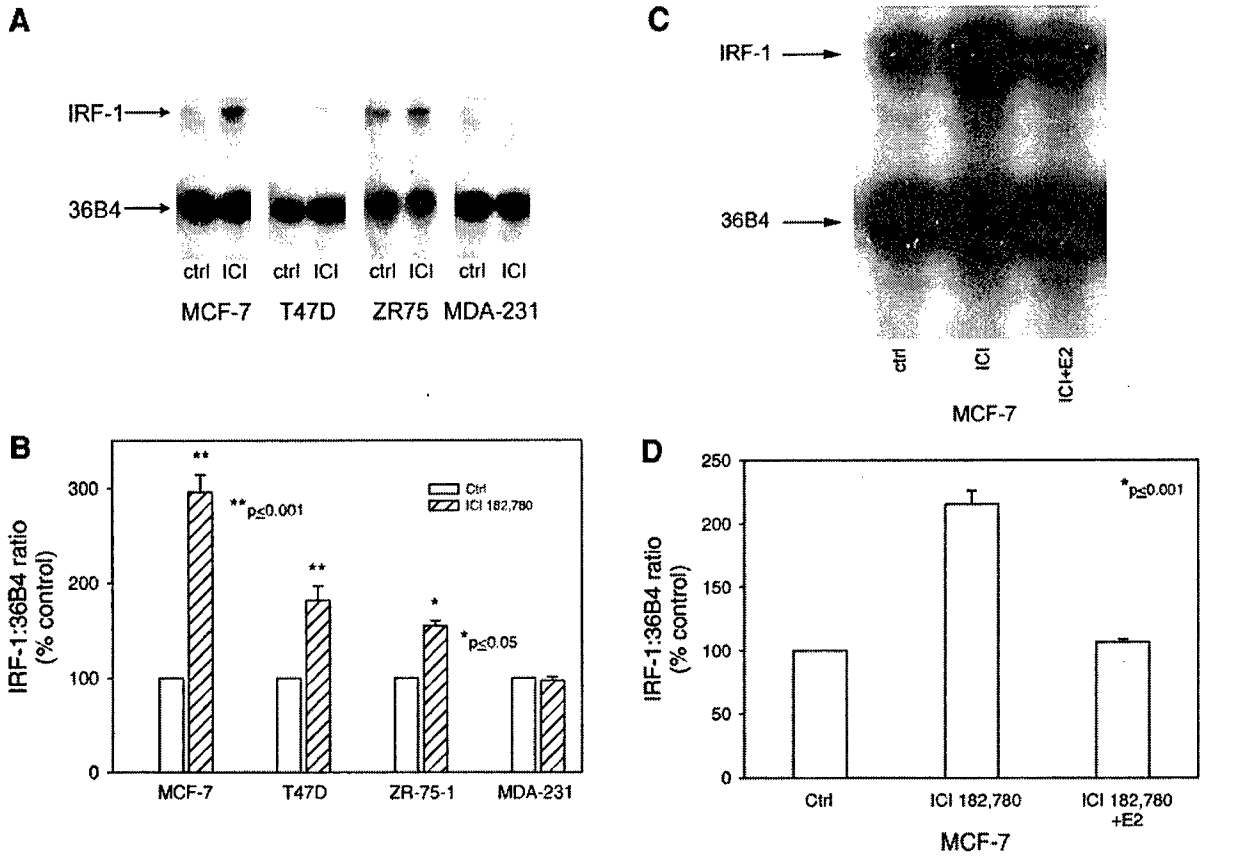

Fig. 2. Endocrine regulation of IRF-1 mRNA transcription in breast cancer cell lines. *A*, representative RNase protection data for IRF-1 mRNA expression. *B*, ICI 182,780 induces IRF-1 mRNA expression in ER+ but not ER− breast cancer cells. Cells were treated with 100 nM ICI 182,780 or ethanol vehicle. Data represent mean ± SE of three determinations, in which absorbance is expressed as a ratio of IRF-1:36B4 and represented as a percentage of vehicle control-treated cells. *, $P \leq 0.001$ for ICI 182,780 *versus* control-treated cells within each cell line for MCF-7 and T47D and $P < 0.05$ for ZR75. $P = 0.880$ for MDA-MB-231; Student's *t* test. *C*, representative RNase protection data for IRF-1 mRNA expression; *D*, estradiol reverses ICI 182,780-induced IRF-1 mRNA transcription in MCF-7 cells. *, $P < 0.001$; Student's *t* test.

dnIRF-1 Does Not Affect ICI 182,780-Induced Changes in Cell Cycle Distribution. Although antiestrogens can affect both cell cycle distribution and the rate of apoptosis, cell proliferation assays measure the sum of these activities. Hence, we asked directly whether the effects of dnIRF-1 on proliferation reflected an inhibition of the ability of ICI 182,780 to arrest cells in G_0-G_1. The data in Fig. 9 show that dnIRF-1 does not affect the ICI 182,780-induced cell cycle arrest in G_0-G_1 in either MCF-7/dnIRF-1 (Fig. 9*A*) or T47D/dnIRF-1 cells (Fig. 9*B*). Thus, the residual antiproliferative effects of ICI 182,780 (Fig. 8) in dnIRF-1-expressing cells are those conferred by cell cycle arrest. These data strongly implicate changes in apoptosis as being the primary mechanism through which dnIRF-1 reduces the antiproliferative effects of ICI 182,780 in MCF-7 and T47D cells.

ICI 182,780-Induced Apoptosis Is Reduced by dnIRF-1. To determine whether the effects of dnIRF-1 on cellular sensitivity to ICI 182,780 are mediated by its ability to influence signaling to apoptosis, the ability of dnIRF-1 to affect ICI 182,780-induced apoptosis was assessed directly by measuring annexin V staining (49, 50). Apoptosis was measured only in those cells expressing the dnIRF-1 transgene or empty vector control (as assessed by EGFP expression), to ensure that any effects were likely to be a direct result of the inhibition of IRF-1. When treated with 100 nM ICI 182,780, 30% of MCF-7 control transfectants undergo apoptosis. Expression of dnIRF-1 significantly reduces this ICI 182,780-induced apoptotic response by >4-fold in MCF-7/dnIRF-1 cells to 7% (Fig. 10; $P < 0.034$). The basal rate of apoptosis, measured in control MCF-7 cells treated with ethanol, is about 5% (Fig. 10). Thus, the full apoptotic response to ICI 182,780 is blocked by dnIRF-1. Studies were also performed in T47D and T47D/dnIRF-1 cells, which unlike MCF-7 cells contain a mutant and nonfunctional p53. T47D/dnIRF-1 cells show a similar 4-fold reduction in the ability of ICI 182,780 to induce apoptosis (not shown). These data with dnIRF-1 in both MCF-7 (wild-type p53) and T47D (mutant p53) strongly suggesting that IRF-1 is a critical mediator of this signal and that its activities are independent of p53.

DISCUSSION

Data from our previous studies demonstrate an association between IRF-1 expression and acquired cross-resistance to antiestrogens (19). We now show that IRF-1 is a key signaling protein involved in mediating the sensitivity of breast cancer cells to ICI 182,780-induced apoptosis. Basal IRF-1 mRNA expression is down-regulated in antiestrogen-resistant cells (both the ER+ MCF7/LCC9 model of acquired resistance and the ER− MDA-MB-231 model of *de novo* resistance). Moreover, the ability of antiestrogens to regulate IRF-1 mRNA transcription is absent in the ER− and lost in the ER+ antiestrogen-resistant cells. The functional relevance of these observations is shown by the ability of dnIRF-1 to reduce significantly the antiproliferative effects of ICI 182,780 in both the antiestrogen-sensitive MCF-7 and T47D cells. Notably, dnIRF-1 does not eliminate basal IRF-1 activity in these cells. Loss of IRF-1 activity could induce confounding compensatory effects unlikely to occur in breast tumors, which appear to retain detectable IRF-1 protein expression (36). Thus, the data reported herein likely reflect the contribution of only the antiestrogen induced IRF-1.

Specificity of these effects, in the context of the signaling of IRF-1

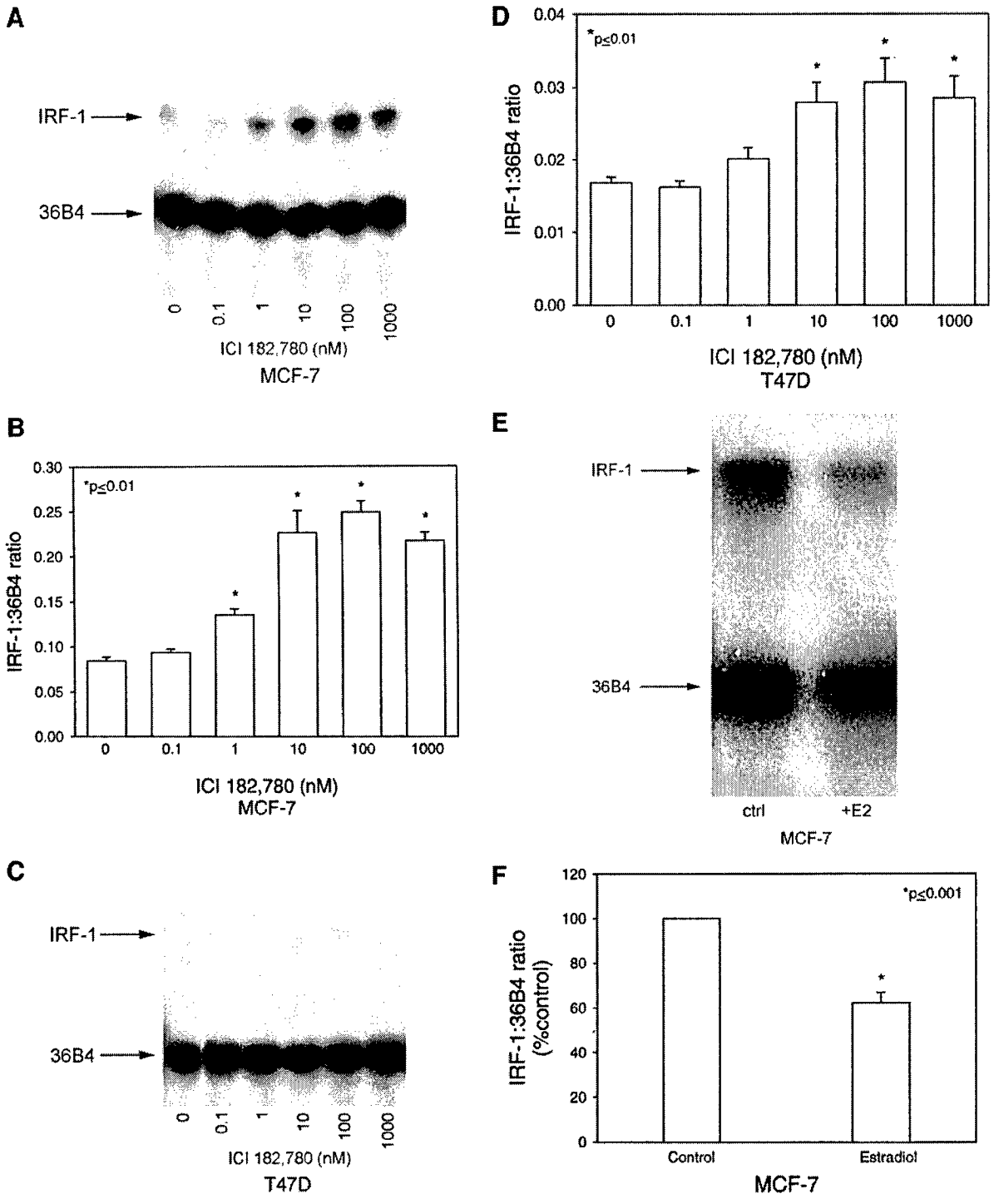

Fig. 3. Dose-response and time-response relationships for the induction of IRF-1 mRNA by ICI 182,780 in MCF-7 (*A* and *B*) and T47D cells (*C* and *D*). *A*, representative RNase protection assay. *36B4*, loading control. *B*, dose-response relationship for IRF-1 mRNA induction in MCF-7 cells. Cells were treated with ICI 182,780 or ethanol vehicle for 72 h. Data represent mean ± SE of three independent replicate experiments, in which absorbance is expressed as a ratio of IRF-1:36B4. *, $P \leq 0.01$ for treatments *versus* control; Dunnett's test. *C*, representative RNase protection assay. *36B4*, loading control. *D*, dose-response relationship for IRF-1 mRNA induction in T47D cells. Cells were treated as in *B*. Data represent mean ± SE of three independent replicate experiments, in which absorbance is expressed as a ratio of IRF-1:36B4. *, $P \leq 0.01$ for treatments *versus* control; Dunnett's test. *E*, representative RNase protection assay. *36B4*, loading control. *F*, estradiol regulation of IRF-1 mRNA expression in MCF-7 cells. Cells were stripped of estrogens, grown in the absence of estrogen (charcoal stripped calf serum-IMEM), and then treated with either 1 nM estradiol or ethanol vehicle for 24 h. Data represent mean ± SE of three independent replicate experiments, in which absorbance is expressed as a ratio of IRF-1:36B4 and represented as a percentage of vehicle control-treated cells. *, $P < 0.001$; Student's *t* test.

in response to ER-mediated events, also is apparent. Estradiol blocks antiestrogen-induced IRF-1 in MCF-7 cells, and no endocrine regulation is seen in ER− cells. Neither the loss of endocrine regulation in MCF7/LCC9 cells nor the absence of its endocrine regulation in MDA-MB-231 cells compromises the ability of doxorubicin to induce IRF-1 in these cells and to inhibit their proliferation (not shown). This latter effect is consistent with patterns of clinical responses to these drugs, because breast cancer patients who are resistant to antiestrogens can respond to cytotoxic chemotherapy.

The ability of dnIRF-1 to block ICI 182,780-induced inhibition of

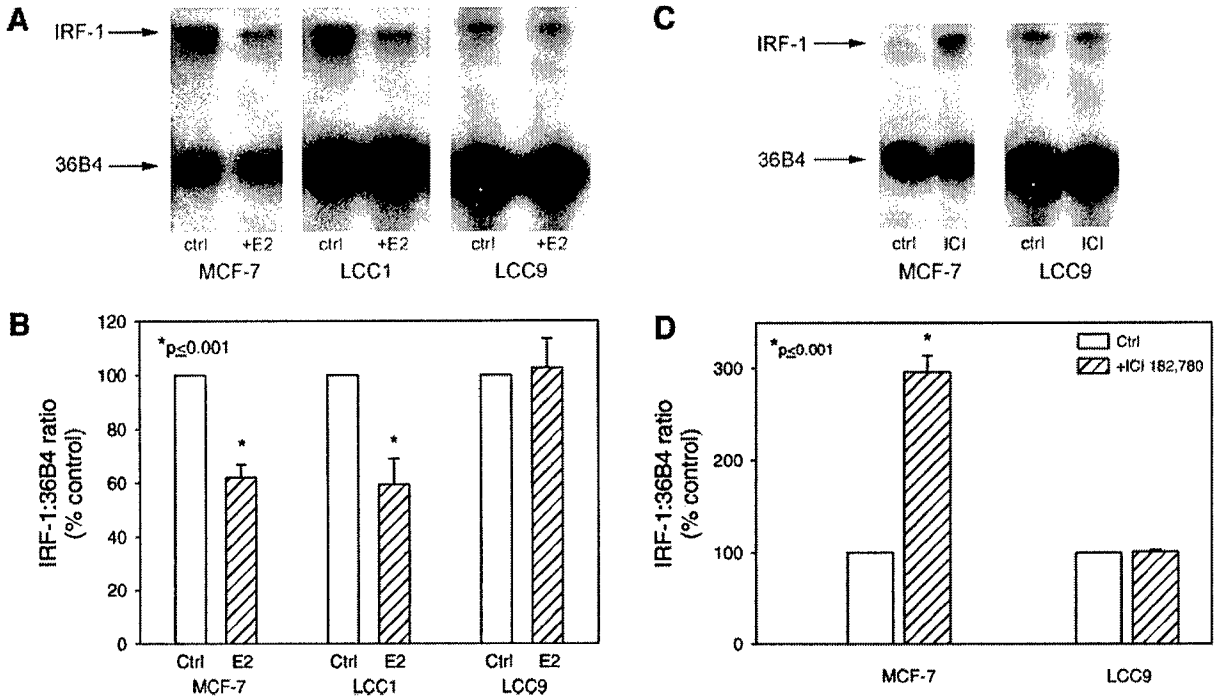

Fig. 4. Hormonal regulation of IRF-1 expression is lost in antiestrogen-resistant cells. *A*, representative RNase protection assay. *36B4*, loading control. *B*, estradiol regulation of IRF-1 mRNA expression. Cells were stripped of estrogens, grown in the absence of estrogen (charcoal stripped calf serum-IMEM), and then treated with either 1 nM estradiol or ethanol vehicle for 24 h. Data represent mean ± SE of three independent replicate experiments, in which absorbance is expressed as a ratio of IRF-1:36B4 and represented as a percentage of vehicle control-treated cells. *, $P \leq 0.001$ for estradiol *versus* control for each of MCF7 and MCF7/LCC1 cells; $P = 0.864$ for estradiol *versus* control-treated MCF-7/LCC9 cells; Student's *t* test. *C*, ICI 182,780 regulation of IRF-1 mRNA expression: representative RNase protection assay. *36B4*, loading control. Cells were treated with 100 nM ICI 182,780 or ethanol vehicle for 72 h. *D*, ICI 182,780 regulation of IRF-1 mRNA expression. Data represent mean ± SE of three determinations, in which absorbance is expressed as a ratio of IRF-1:36B4 and represented as a percentage of vehicle control-treated cells. *, $P \leq 0.001$ for ICI 182,780 *versus* control-treated MCF-7 cells; $P = 0.971$ for ICI 182,780 *versus* control-treated MCF7/LCC9 cells; Student's *t* test.

cell proliferation in MCF-7/dnIRF-1 and T47D/dnIRF-1 cells could reflect changes in the effects of ICI 182,780 on cell cycle and/or apoptosis. However, dnIRF-1 does not affect ICI 182,780-induced cell cycle arrest when expressed in either MCF-7 or T47D cells. In marked contrast, dnIRF-1 effectively eliminates ICI 182,780-induced apoptosis in both MCF-7/dnIRF-1 and T47D/dnIRF-1 cells. Thus, we can separate cell cycle arrest from apoptosis and attribute a significant component of antiestrogen-induced apoptotic signaling to IRF-1. Because dnIRF-1 abrogates ICI 182,780-induced apoptosis (Fig. 10) while enhancing cell growth by approximately 50% (Fig. 8), apoptosis and cell cycle arrest likely contribute equally to the apparent antiproliferative effects of ICI 182,780.

Functionally separating antiestrogen-induced apoptosis from antiestrogen-induced growth arrest has several important implications. Novel therapeutic approaches designed to increase the proapoptotic effects of antiestrogens may be an effective means to improve their ability to increase overall survival in patients because this should increase the proportion of cells undergoing apoptotic cell death. Modalities that increase only the ability of antiestrogens to induce a cell cycle arrest will likely be a less effective strategy. For example, many arrested cells will survive and thereby have more opportunities to adapt, acquire resistance, and generate subsequent disease recurrence. Measuring basal IRF-1 expression and/or the ability of an antiestrogen to induce IRF-1 in the neoadjuvant setting may improve the prediction of endocrine responsiveness. Currently, we incorrectly predict antiestrogen sensitivity in 66% of ER+/progesterone receptor-negative, 55% of ER−/progesterone receptor-positive, and 25% of ER+/progesterone receptor-positive tumors (6).

The ability of IRF-1 to induce growth arrest is associated with the induction of various genes including p53-dependent and -independent events (26, 27) and interactions that may include $p21^{waf1/cip1}$ (26).

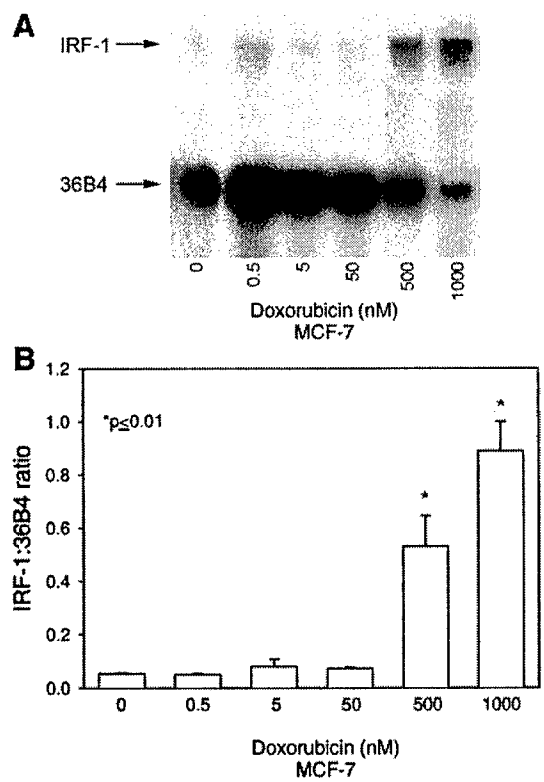

Fig. 5. Doxorubicin induction of IRF-1 mRNA expression. *A*, representative RNase protection assay. *36B4*, loading control. *B*, MCF-7 cells were treated with 1 μM doxorubicin. Data represent mean ± SE of three determinations, in which absorbance is expressed as a ratio of IRF-1:36B4. *, $P \leq 0.01$; Dunnett's test.

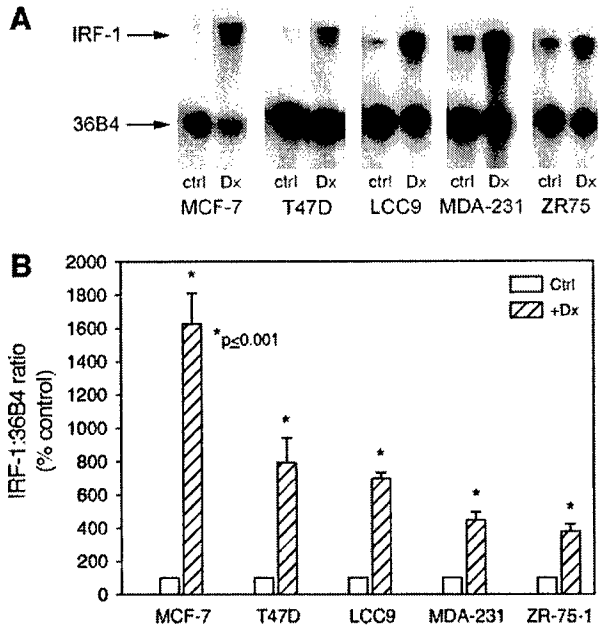

Fig. 6. Doxorubicin induces IRF-1 mRNA expression in both ER+ and ER− breast cancer cell lines. RNase protection assay of ER+ MCF-7, T47D, MCF-7/LCC9, and ZR75 cells and ER− MDA-MB-231 cells treated with 1 μM doxorubicin (*DX*) for 24 h. *A*, representative data from RNase protection assay; *B*, graphical representation of RNase protection assays of ER+ and ER− breast cancer cell lines treated with doxorubicin. Data represent mean ± SE of three independent determinations, in which absorbance is expressed as a ratio of IRF-1:36B4 and represented as a percentage of vehicle control-treated cells. **, $P \leq 0.001$ for doxorubicin *versus* control-treated cells within each cell line for MCF-7 and MCF-7/LCC9 cells; *, $P \leq 0.05$ for MDA-MB-231 cells; Student's *t* test.

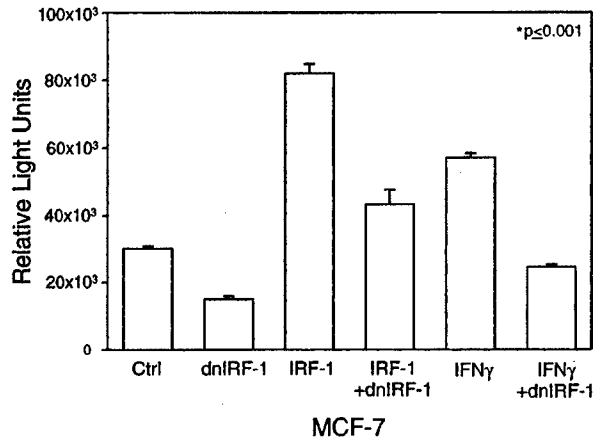

Fig. 7. Inhibition of basal and IFN-γ stimulated ISRE activity by dnIRF-1 in MCF-7 cells. Data represent mean ± SE (representative experiment of four independent replicates), in which data are represented by relative light units. Where appropriate, MCF-7 cells were treated with 500 IU of IFN-γ. *, $P \leq 0.001$ for all transfections *versus* control; Dunnett's test.

Interactions requiring both $p21^{waf1/cip1}$ and p53 may not be central components in antiestrogen signaling through IRF-1. Nonetheless, preliminary data suggest an increase in $p21^{waf1/cip1}$ mRNA expression after ICI 182,780 treatment in MCF-7 and T47D cells (2.91 ± 0.89-fold), consistent with both a previous report on $p21^{waf1/cip1}$ regulation by ICI 182,780 (56) and activation of IRF-1. MCF-7 cells express wild-type p53, whereas T47D cells express a mutant and nonfunctional p53 (57), but both cell lines are responsive to antiestrogen-induced apoptosis in a manner that remains sensitive to the effects of dnIRF-1. However, a role for $p53/p21^{waf1/cip1}$ signaling in the cell cycle effects of antiestrogens cannot be excluded.

The ability of ICI 182,780 to induce apoptosis through IRF-1 activity is likely mediated through changes in caspase activation. IRF-1 can induce several caspases (27, 29, 30), and inhibition of caspase activity blocks antiestrogen-induced apoptosis (58). A specific requirement for caspase-3 seems unlikely because this caspase is not expressed in MCF-7 cells (59). IRF-1 signaling through caspase-1 (27), caspase-7 (29), and caspase-8 (30) is strongly implicated. For example, IRF-1 induces caspase-1 (60), which can regulate apoptosis in normal mammary epithelial cells (61). Overexpression of caspase-1 is lethal in MCF-7 cells (62). Caspase-7 is expressed in MCF-7 cells and may substitute for the loss of caspase-3 in these cells (63). IFN-γ, which induces IRF-1 activity in MCF-7 cells (Fig. 7), is reported to sensitize both MCF-7 and MDA-MB-231 cells to apoptosis through inducing caspase-8 (64). TAM can induce caspase-8 (58), and consistent with our observations in T47D cells, caspase-8-induced apoptosis occurs independent of p53 (64). Studies to determine which caspases are functionally involved in IRF-1 signaling in breast cancer are currently in progress.

Although data in this study show reduced IRF-1 expression and loss of its endocrine regulation in antiestrogen-resistant cells, the level of IRF-1 activity in cells is also affected by protein-protein interactions with the nucleolar phosphoprotein nucleophosmin (NPM; Ref. 65). Not previously reported in breast cancer cells, we now have preliminary data to suggest that this functional interaction also occurs in T47D cells (not shown). NPM is an estrogen-induced protein in

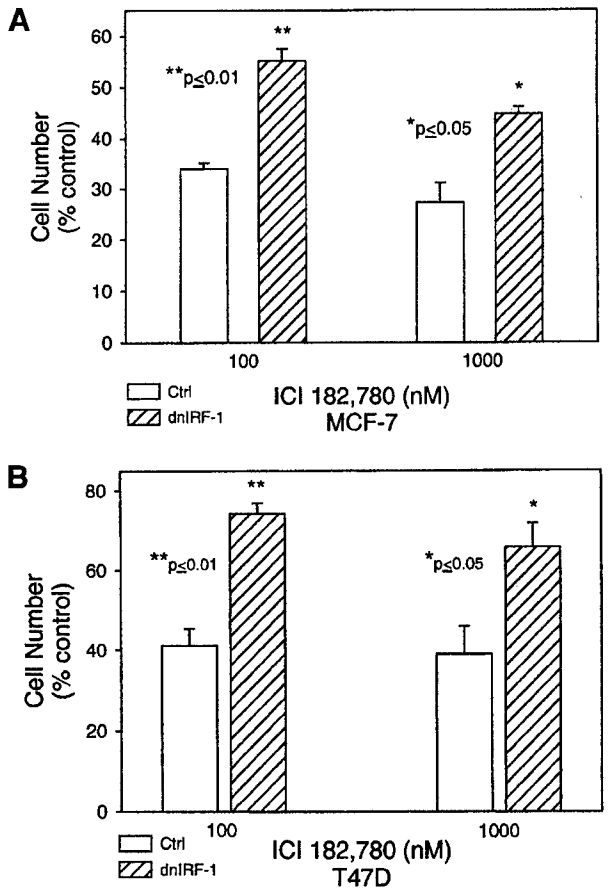

Fig. 8. Inhibition of ICI 182,780 effects on cell proliferation by dnIRF-1. *A*, MCF-7 cells with and without constitutive dnIRF-1 expression. *B*, T47D cells with and without constitutive dnIRF-1 expression. For each cell line, cells were treated with ethanol vehicle, 100 nM ICI 182,780 or 1 μM ICI 182,780 for 3 days. Data represent mean ± SE of three determinations. *, $P = 0.002$, MCF-7 100 nM ICI 182,780; $P = 0.013$, MCF-7 1 μM ICI 182,780; Student's *t* test. $P = 0.002$, T47D 100 nM ICI 182,780; $P = 0.043$, T47D 1 μM ICI 182,780; Student's *t* test.

MCF-7 cells that is down-regulated by antiestrogens (66), and its expression is increased in MCF-7/LCC9 when compared with MCF-7/LCC1 cells (19). Thus, in addition to down-regulating IRF-1 mRNA expression, antiestrogen-resistant cells have up-regulated expression of an endogenous inhibitor (NPM). Interestingly, we have previously shown that NPM autoantibody levels are lower in TAM-treated patients, suggesting that NPM/IRF-1 interactions also may be clinically relevant (67).

It seems likely that an acquired antiestrogen resistance phenotype is conferred not by the alteration of a single gene or signal transduction pathway but rather through the perturbation of a signaling network of integrated signaling pathways (15). The data presented here are consistent with cell signaling through IRF-1 being a key component or node in such a signaling network. Activity as a signaling node is implied by (*a*) the potential for diversity/redundancy of signaling to a key end point (apoptosis) downstream of IRF-1 (cooperation with p53, $p21^{waf1/cip1}$, and regulation of several caspases); (*b*) the redundancy apparent in regulating IRF-1 activity (down-regulation of basal transcription, loss of ER-mediated transcription, and concurrent up-regulation of the endogenous inhibitor NPM); (*c*) the apparent specificity for antiestrogen resistance (cytotoxic drugs can induce IRF-1 in antiestrogen-resistant cells); and (*d*) the altered regulation of IRF-1 activity/expression in models of both *de novo* and acquired antiestrogen resistance. This node may be important in affecting other signals in breast cancer cells. For example, IRF-1 is downstream of tumor necrosis factor signaling, and both tumor necrosis factor α and its receptor tumor necrosis factor R1 are down-regulated in MCF7/LCC9 cells, implying a cross-resistance to tumor necrosis factor-mediated events (15, 19).

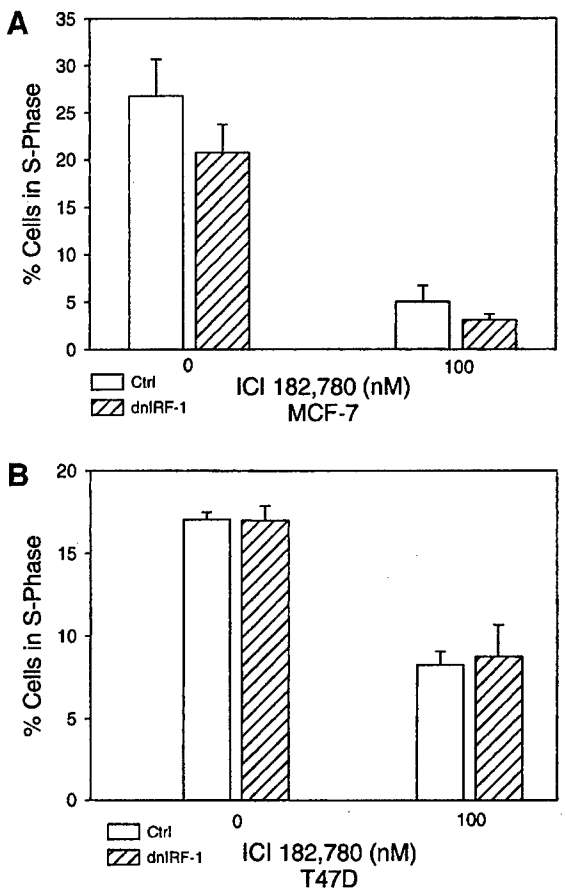

Fig. 9. Expression of dnIRF-1 does not affect ICI 182,780-induced changes in cell cycle distribution. *A*, MCF-7 cells with and without constitutive dnIRF-1 expression; *B*, T47D cells with and without constitutive dnIRF-1 expression. For each cell line, cells were treated with either ethanol vehicle or 100 nM ICI 182,780 for 3 days. Data represent mean ± SE of three determinations. *, $P = 0.40$, MCF-7 0 nM ICI 182,780 (vehicle control); $P = 0.237$, MCF-7 100 nM ICI 182,780; Student's *t* test. $P = 0.962$, T47D 0 nM ICI 182,780; $P = 0.836$, T47D 100 nM; Student's *t* test.

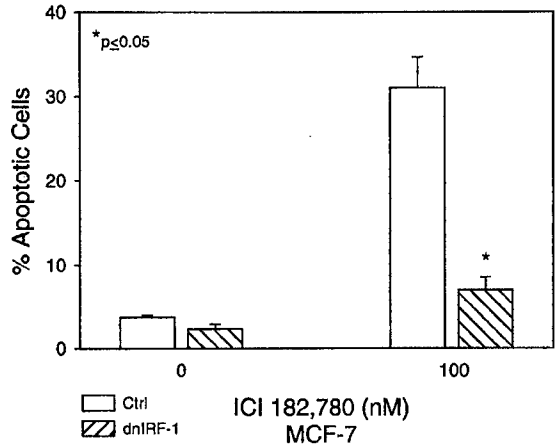

Fig. 10. ICI 182,780-induced apoptosis is reduced by dnIRF-1 expression. MCF-7 cells with and without constitutive dnIRF-1 expression. Data represent mean ± SE of three independent replicate experiments. dnIRF-1- and control-transfected cells were treated with either ethanol vehicle or 100 nM ICI 182,780 for 3 days. Annexin V analysis was measured by FACS. *, $P \leq 0.05$ for ICI 182,780-treated control transfectants *versus* dnIRF-1 transfectants (Dunnett's test).

The ability of doxorubicin to induce IRF-1 in antiestrogen-resistant cells and to inhibit proliferation in these cells is a clinically relevant phenotype. We and others (36, 68) have detected IRF-1 expression by immunohistochemistry in breast cancer specimens, this pattern of expression being consistent with a potential tumor suppressor role for IRF-1 (21, 36). Our preliminary data suggest that the pattern of IRF-1 expression in breast cancers, as measured by immunohistochemistry, is consistent with other components of our network. For example, we detect an inverse pattern of expression between IRF-1 and nuclear factor κB as seen in MCF7/LCC1 *versus* MCF7/LCC9 cells (19, 68). These observations may ultimately lead to a better ability to identify patients that will respond to antiestrogens and to predict which patients will ultimately develop antiestrogen resistance. Interfering with the putative "IRF-1 node" may allow for the development of novel therapeutic strategies in endocrine-resistant breast cancers.

ACKNOWLEDGMENTS

Technical services were provided by the Flow Cytometry & Cell Sorting and Macromolecular Shared Resources.

REFERENCES

1. Early Breast Cancer Trialists' Collaborative Group. Tamoxifen for early breast cancer: an overview of the randomized trials. Lancet 1998;351:1451–67.
2. Early Breast Cancer Trialists' Collaborative Group. Systemic treatment of early breast cancer by hormonal, cytotoxic, or immune therapy. Lancet 1992;399:1–15.
3. Winer EP, Hudis C, Burstein HJ, et al. American Society of Clinical Oncology technology assessment on the use of aromatase inhibitors as adjuvant therapy for women with hormone receptor-positive breast cancer: status report 2002. J Clin Oncol 2002;20:3317–27.
4. Ravdin P. Aromatase inhibitors for the endocrine adjuvant treatment of breast cancer. Lancet 2002;359:2126–7.
5. Chlebowski RT, Col N, Winer EP, et al. American Society of Clinical Oncology technology assessment of pharmacologic interventions for breast cancer risk reduction including tamoxifen, raloxifene, and aromatase inhibition. J Clin Oncol 2002; 20:3328–43.
6. Clarke R, Leonessa F, Welch JN, Skaar TC. Cellular and molecular pharmacology of antiestrogen action and resistance. Pharmacol Rev 2001;53:25–71.
7. Robertson JFR. ICI 182,780 (Fulvestrant): the first oestrogen receptor down-regulator: current clinical data. Br J Cancer 2001;85(Suppl 2):11–14.

8. Howell A, DeFriend D, Robertson JFR, Blamey RW, Walton P. Response to a specific antioestrogen (ICI 182,780) in tamoxifen-resistant breast cancer. Lancet 1995;345:29–30.
9. Howell A, Robertson JF, Quaresma AJ, et al. Fulvestrant, formerly ICI 182.780, is as effective as anastrozole in postmenopausal women with advanced breast cancer progressing after prior endocrine treatment. J Clin Oncol 2002;20:3396–403.
10. Osborne CK, Pippen J, Jones SE, et al. Double-blind, randomized trial comparing the efficacy and tolerability of fulvestrant versus anastrozole in postmenopausal women with advanced breast cancer progressing on prior endocrine therapy: results of a North American trial. J Clin Oncol 2002:20:3386–95.
11. Wakeling AE. The future of new pure antiestrogens in clinical breast cancer. Breast Cancer Res Treat 1993;25:1–9.
12. Dauvois S, Danielian PS, White R, Parker MG. Antiestrogen ICI 164,384 reduces cellular estrogen receptor content by increasing its turnover. Proc Natl Acad Sci USA 1992;89:4037–41.
13. Fawell SE, White R, Hoare S, Sydenham M, Page M, Parker MG. Inhibition of estrogen receptor-DNA binding by the "pure" antiestrogen ICI 164,384 appears to be mediated by impaired receptor dimerization. Proc Natl Acad Sci USA 1990;87:6883–7.
14. Wakeling AE, Bowler J. Novel antioestrogens without partial agonist activity. J Steroid Biochem 1988;31:645–53.
15. Clarke R, Liu M, Bouker KB, et al. Antiestrogen resistance in breast cancer and the role of estrogen receptor signaling. Oncogene 2003;22:7316–39.
16. Fisher B, Costantino JP, Wickerham DL, et al. Tamoxifen for prevention of breast cancer: report of the National Surgical Adjuvant Breast and Bowel Project P-1 study. J Natl Cancer Inst (Bethesda) 1998;90:1371–88.
17. Veronesi U, Maisonneuve P, Rotmensz N, et al. Italian randomized trial among women with hysterectomy: tamoxifen and hormone-dependent breast cancer in high-risk women. J Natl Cancer Inst (Bethesda) 2003;95:160–5.
18. Clarke R, Brünner N. Acquired estrogen independence and antiestrogen resistance in breast cancer: estrogen receptor-driven phenotypes? Trends Endocrinol Metab 1996; 7:25–35.
19. Gu Z, Lee RY, Skaar TC, et al. Association of interferon regulatory factor-1, nucleophosmin, nuclear factor-κB, and cyclic AMP response element binding with acquired resistance to Faslodex (ICI 182,780). Cancer Res 2002;62:3428–37.
20. Tanaka N, Ishihara M, Kitagawa M, et al. Cellular commitment to oncogene-induced transformation or apoptosis is dependent on the transcription factor IRF-1. Cell 1994;77:829–39.
21. Tanaka N, Ishihara M, Taniguchi T. Suppression of c-myc or fosB-induced cell transformation by the transcription factor IRF-1. Cancer Lett 1994;83:191–6.
22. Yim JH, Wu SJ, Casey MJ, Norton JA, Doherty GM. IFN regulatory factor-1 gene transfer into an aggressive, nonimmunogenic sarcoma suppresses the malignant phenotype and enhances immunogenicity in syngeneic mice. Hokkaido Igaku Zasshi 1997;71:509–16.
23. Sillman CL, Sever CE, Pallavicini MG, et al. Deletion of IRF-1, mapping to chromosome 5q31.1, in human leukemia and preleukemic myelodysplasia. Science 1993;259:968–70.
24. Tamura G, Ogasawara S, Hishizuka S, et al. Two distinct regions of deletion on the long arm of chromosome 5 in differentiated adenocarcinomas of the stomach. Cancer Res 1996;56:612–5.
25. Nozawa H, Oda E, Nakao K, et al. Loss of transcription factor IRF-1 affects tumor susceptibility in mice carrying the Ha-ras transgene or nullizygosity for p53. Genes Dev 1999;1–3:1240–5.
26. Tanaka N, Ishihara M, Lamphier MS, et al. Cooperation of the tumour suppressors IRF-1 and p53 in response to DNA damage. Nature 1996;382:816–818.
27. Tamura T, Ishihara M, Lamphier MS, et al. An IRF-1-dependent pathway of DNA damage-induced apoptosis in mitogen-activated T lymphocytes. Nature 1995;376: 596–9.
28. Moro A, Santos A, Arana MJ, Perea SE. Activation of the human p27(Kip1) promoter by IFNα 2b. Biochem Biophys Res Commun 2000;269:31–4.
29. Sanceau J, Hiscott J, Delattre O, Wietzerbin J. IFN-β induces serine phosphorylation of Stat-1 in Ewing's sarcoma cells and mediates apoptosis via induction of IRF-1 and activation of caspase-7. Oncogene 2000;19:3372–83.
30. Suk K, Chang I, Kim Y, et al. Interferon γ (IFNγ) and tumor necrosis factor α synergism in ME-180 cervical cancer cell apoptosis and necrosis: IFNγ inhibits cytoprotective NF-κB through STAT1/IRF-1 pathways. J Biol Chem 2001;276: 13153–9.
31. Chow W, Fang J, Yee J. The IFN regulatory factor family participates in regulation of Fas ligand gene expression in T cells. J Immunol 2000;164:3512–8.
32. Elledge RM, Allred DC. The p53 tumor suppressor gene in breast cancer. Breast Cancer Res Treat 1994;32:39–47.
33. Early Breast Cancer Trialists' Collaborative Group. Polychemotherapy for early breast cancer: an overview of randomised trials. Lancet 1998;352:930–42.
34. Berry D, Muss H, Thor A, et al. HER-2/neu and p53 expression versus tamoxifen resistance in estrogen receptor-positive, node-negative breast cancer. J Clin Oncol 2000;18:3471–9.
35. Harroch S, Revel M, Chebath J. Induction by interleukin-6 of interferon regulatory factor 1 (IRF-1) gene expression through the palindromic interferon response element pIRE and cell type-dependent control of IRF-1 binding to DNA. EMBO J 1994;13: 1942–9.
36. Doherty GM, Boucher L, Sorenson K, Lowney J. Interferon regulatory factor expression in human breast cancer. Ann Surg 2001;233:623–9.
37. Brooks SC, Locke ER, Soule HD. Estrogen receptor in a human cell line (MCF-7) from breast carcinoma. J Biol Chem 1973;248:6251–3.
38. Chalbos D, Vignon F, Keydar I, Rochefort H. Estrogens stimulate cell proliferation and induce secretory proteins in a human breast cancer cell line (T47D). J Clin Endocrinol Metab 1982;55:276.
39. Brünner N, Boulay V, Fojo A, Freter C, Lippman ME, Clarke R. Acquisition of hormone-independent growth in MCF-7 cells is accompanied by increased expression of estrogen-regulated genes but without detectable DNA amplifications. Cancer Res 1993;53:283–90.
40. Brünner N, Boysen B, Jirus S, et al. MCF7/LCC9: an antiestrogen resistant MCF-7 variant in which acquired resistance to the steroidal antiestrogen ICI 182,780 confers an early crossresistance to the non-steroidal antiestrogen tamoxifen. Cancer Res 1997;57:3486–93.
41. Pratt MAC, Bishop TE, White D, et al. Estrogen withdrawal-induced NF-κB activity and bcl-3 expression in breast cancer cells: roles in growth and hormone independence. Mol Cell Biol 2003;23:6887–900.
42. Fisher B, Dignam J, Bryant J, Wolmark N. Five versus more than five years of tamoxifen for lymph node-negative breast cancer: updated findings from the National Surgical Adjuvant Breast and Bowel Project B-14 randomized trial. J Natl Cancer Inst (Bethesda) 2001;93:684–90.
43. Clarke R, Brünner N, Katzenellenbogen BS, et al. Progression from hormone dependent to hormone independent growth in MCF-7 human breast cancer cells. Proc Natl Acad Sci USA 1989;86:3649–53.
44. LaBorda J. 36B4 cDNA used as an estradiol-independent mRNA control is the cDNA for human acidic ribosomal phosphoprotein PO. Nucleic Acids Res 1991;19:3998.
45. Clarke R, Brünner N, Katz D, et al. The effects of a constitutive production of TGF-α on the growth of MCF-7 human breast cancer cells in vitro and in vivo. Mol Endocrinol 1989;3:372–80.
46. Sledz CA, Holko M, De Veer MJ, Silverman RH, Williams BR. Activation of the interferon system by short-interfering RNAs. Nat Cell Biol 2003;5:834–9.
47. Bridge AJ, Pebernard S, Ducraux A, Nicoulaz AL, Iggo R. Induction of an interferon response by RNAi vectors in mammalian cells. Nat Genet 2003;34:263–4.
48. Vindelov LL, Christensen IJ, Nissen NI. A detergent-trypsin method for the preparation of nuclei for flow cytometric DNA analysis. Cytometry 1983;3:323–7.
49. Lindner DJ, Ma X, Hu J, Karra S, Kalvakolanu DV. Thioredoxin reductase plays a critical role in IFN retinoid-mediated tumor-growth control in vivo. Clin Cancer Res 2002;8:3210–8.
50. Del Bino G, Darzynkiewicz Z, Degraef C, Mosselmans R, Fokan D, Galand P. Comparison of methods based on annexin-V binding, DNA content or TUNEL for evaluating cell death in HL-60 and adherent MCF-7 cells. Cell Prolif 1999;32:25–37.
51. Gad S and Weil CS. Statistics and experimental design for toxicologists. Caldwell, NJ: Telford Press; 1988.
52. Kano A, Haruyama T, Akaike T, Watanabe Y. IRF-1 is an essential mediator in IFN-γ-induced cell cycle arrest and apoptosis of primary cultured hepatocytes. Biochem Biophys Res Commun 1999;257:672–7.
53. Howell A, DeFriend DJ, Robertson JFR, et al. Pharmacokinetics, pharmacological and anti-tumor effects of the specific anti-oestrogen ICI 182780 in women with advanced breast cancer. Br J Cancer 1996;74:300–8.
54. Paik S, Bryant J, Park C, et al. ErbB-2 and response to doxorubicin in patients with axillary lymph node-positive, hormone receptor-negative breast cancer. J Natl Cancer Inst (Bethesda) 1998:90:1361–70.
55. Trock BJ, Leonessa F, Clarke R. Multidrug resistance in breast cancer: a meta analysis of MDR1/gp170 expression and its possible functional significance. J Natl Cancer Inst (Bethesda) 1997;89:917–31.
56. Carroll JS, Prall OW, Musgrove EA, Sutherland RL. A pure estrogen antagonist inhibits cyclin E-Cdk2 activity in MCF-7 breast cancer cells and induces accumulation of p130–E2F4 complexes characteristic of quiescence. J Biol Chem 2000;275: 38221–9.
57. Bartek J, Iggo R, Gannon J, Lane DP. Genetic and immunochemical analysis of mutant p53 in human breast cancer cell lines. Oncogene 1990;5:893–9.
58. Mandlekar S, Hebbar V, Christov K, Kong AN. Pharmacodynamics of tamoxifen and its 4-hydroxy and N-desmethyl metabolites: activation of caspases and induction of apoptosis in rat mammary tumors and in human breast cancer cell lines. Cancer Res 2000:60:6601–6.
59. Kurokawa H, Nishio K, Fukumoto H, et al. Alteration of caspase-3 (CPP32/Yama/apopain) in wild-type MCF-7, breast cancer cells. Oncol Rep 1999;6:33–7.
60. Tamura T, Ueda S, Yoshida M, Matsuzaki M, Mohri H, Okubo T. Interferon-γ induces ICE gene expression and enhances cellular susceptibility to apoptosis in the U937 leukemia cell line. Biochem Biophys Res Commun 1996;229:21–6.
61. Boudreau N, Sympson CJ, Werb Z, Bissell MJ. Suppression of ICE and apoptosis in mammary epithelial cells by extracellular matrix. Science 1995;267:891–3.
62. Keane MM, Ettenberg SA, Lowrey GA, Russell EK, Lipkowitz S. Fas expression and function in normal and malignant breast cell lines. Cancer Res 1996;56:4791–8.
63. Liang Y, Yan C, Schor NF. Apoptosis in the absence of caspase 3. Oncogene 2001;20:6570–8.
64. Ruiz-Ruiz C, Munoz-Pinedo C, Lopez-Rivas A. Interferon-γ treatment elevates caspase-8 expression and sensitizes human breast tumor cells to a death receptor-induced mitochondria-operated apoptotic program. Cancer Res 2000;60:5673–80.
65. Kondo T, Minamino N, Nagamura-Inoue T, Matsumoto M, Taniguchi T, Tanaka N. Identification and characterization of nucleophosmin/B23/numatrin which binds the anti-oncogenic transcription factor IRF-1 and manifests oncogenic activity. Oncogene 1997;15:1275–81.
66. Skaar TC, Prasad SC, Sharaeh S, Lippman ME, Brunner N, Clarke R. Two-dimensional gel electrophoresis analyses identify nucleophosmin as an estrogen regulated protein associated with acquired estrogen-independence in human breast cancer cells. J Steroid Biochem Mol Biol 1998;67:391–402.
67. Brankin B, Skaar TC, Trock BJ, Berris M, Clarke R. Autoantibodies to numatrin: an early predictor for relapse in breast cancer. Cancer Epidemiol Biomark Prev 1998;7:1109–15.
68. Zhu Y, Bouker KB, Skaar TC, et al. High throughput tissue microarray study of antiestrogen related genes in human breast cancers [abstract]. In: Proceedings of the 85th Annual Meeting of the Endocrine Society 2003; p.140.

The nuclear factor κB inhibitor parthenolide restores ICI 182,780 (Faslodex; fulvestrant)–induced apoptosis in antiestrogen-resistant breast cancer cells

Rebecca B. Riggins, Alan Zwart, Ruchi Nehra, and Robert Clarke

Lombardi Comprehensive Cancer Center and Department of Oncology, Georgetown University School of Medicine, Washington, District Columbia

Abstract

The molecular mechanisms underlying the acquisition of resistance to the antiestrogen Faslodex are poorly understood, although enhanced expression and activity of nuclear factor κB (NFκB) have been implicated as a critical element of this phenotype. The purpose of this study was to elucidate the mechanism by which NFκB up-regulation contributes to Faslodex resistance and to determine whether pharmacologic inhibition of NFκB by the small molecule parthenolide could restore Faslodex-mediated suppression of cell growth. Basal expression of multiple NFκB-related molecules in MCF7-derived LCC1 (antiestrogen-sensitive) and LCC9 (antiestrogen-resistant) breast cancer cells was determined, and cells were treated with Faslodex or parthenolide. The effect of these drugs either singly or in combination was assessed by cell proliferation, estrogen receptor (ER)–dependent transcriptional activation, cell cycle analysis, and apoptosis assays. Expression of the p65 NFκB subunit and the upstream NFκB regulator IκB kinase γ/NFκB essential modulator were increased in the resistant MCF7/LCC9 cells (P = 0.001 and 0.04, respectively). Whereas MCF7/LCC9 cells were unresponsive to Faslodex alone, parthenolide effectively inhibited MCF7/LCC9 cell proliferation and the combination of Faslodex and parthenolide resulted in a 4-fold synergistic reduction in cell growth (P = 0.03). This corresponded to a restoration of Faslodex-induced apoptosis (P = 0.001), with no observable changes in ER-dependent transcription or cell cycle phase distribution. Because parthenolide has shown safety in Phase I clinical trials, these findings have direct clinical relevance and provide support for the design of clinical studies combining antiestrogens and parthenolide in ER-positive breast cancer. [Mol Cancer Ther 2005; 4(1):33–41]

Introduction

Antiestrogens inhibit the function of the estrogen receptor (ER), a nuclear transcription factor that directs the expression of genes that contribute to proliferation and cell growth (reviewed in refs. 1, 2). The most frequently prescribed is the nonsteroidal antiestrogen tamoxifen, which has been shown to be highly effective in both the treatment of ER-positive breast tumors and in reducing breast cancer incidence in women at high risk for the disease. However, most ER-positive tumors become estrogen independent and develop resistance to antiestrogen therapy, whereas the remainder (~30%) exhibit *de novo* or intrinsic resistance. Once resistance has developed, treatment with most nonsteroidal antiestrogens is usually unsuccessful.

In contrast, the steroidal antiestrogen Faslodex (ICI 182,780; ICI) induces significant clinical responses in patients whose tumors have acquired tamoxifen resistance (3). The effectiveness of Faslodex in patients with tamoxifen-resistant disease is similar to that of the aromatase inhibitor anastrozole, and several clinical trials have shown that Faslodex may be a viable alternative to nonsteroidal antiestrogens and aromatase inhibitors as a first-line endocrine treatment (4). Faslodex stimulates degradation of the ER and prevents receptor dimerization, inhibiting estrogen-dependent gene transcription (5, 6). As a pure antagonist of the ER, Faslodex is not associated with the increased risk for endometrial cancer that is seen with tamoxifen (7).

The antiestrogen resistance phenotype is complex, involving many changes at the cellular and molecular levels. Antiestrogens are cytostatic, inducing a G_0-G_1 block in breast cancer cells in culture (1, 8). However, these drugs are also capable of actively inducing programmed cell death or apoptosis, which is consistent with the ability of antiestrogens to increase overall survival (9). One way in which breast cancer cells may become antiestrogen resistant is through changes in gene networks that control cell proliferation and apoptosis (10). To test this hypothesis,

Received 8/4/04; revised 10/28/04; accepted 11/10/04.

Grant support: Public Health Service awards R01-CA/AG58022-10 (R. Clarke); Institutional Training grant T32A09686 (Georgetown University; R. Riggins); Department of Defense awards BC031348 (R. Nehra), BC010619, and BC990358 (R. Clarke) from the United States Army Medical Research and Materiel Command; technical services provided by the Flow Cytometry and Cell Sorting and Microscopy and Imaging Shared Resources funded through Public Health Service awards 2P30-CA-51008 and 1S10 RR15768-01 (Lombardi Comprehensive Cancer Center support grant).

The costs of publication of this article were defrayed in part by the payment of page charges. This article must therefore be hereby marked advertisement in accordance with 18 U.S.C. Section 1734 solely to indicate this fact.

Requests for reprints: Robert Clarke, Lombardi Comprehensive Cancer Center, Georgetown University School of Medicine, Room W405A Research Building, 3970 Reservoir Road NW, Washington, DC 20057. Phone: 202-687-3755; Fax: 202-687-7505.
E-mail: clarker@georgetown.edu

we developed several variant cell lines from the estrogen-dependent and antiestrogen-sensitive MCF-7 breast cancer cells (11, 12). MCF7/LCC1 cells are estrogen independent but remain responsive to antiestrogens; MCF7/LCC9 cells are derivatives of MCF7/LCC1 that have acquired resistance to Faslodex. Similar to what has been observed in breast cancer patients, MCF7/LCC9 cells are cross-resistant to the nonsteroidal antiestrogen tamoxifen (2).

Several genes were found to be altered in the resistant MCF7/LCC9 cells, when their transcriptomes were compared with that of their antiestrogen-sensitive MCF7/LCC1 parental cells by serial analysis of gene expression and microarray analysis (10). For example, we implicated loss of the putative tumor suppressor interferon regulatory factor-1 (IRFI) in acquired resistance and have recently shown IRFI to be a key mediator of the proapoptotic effects of Faslodex in MCF-7 cells (13).

Altered expression of the p65/RelA member of the nuclear factor κB (NFκB) transcription factor family, which can form functional heterodimers with IFN regulatory factor-1 (14), also was strongly implicated in acquired Faslodex resistance. mRNA levels of p65/RelA are up-regulated 2-fold in the MCF7/LCC9 cells, NFκB-dependent transcription are increased 10-fold, and MCF7/LCC9 cells exhibit a greater sensitivity to the growth inhibitory effects of parthenolide, a small molecule inhibitor of NFκB (10). These data strongly but indirectly implicate NFκB action in acquired antiestrogen resistance.

The NFκB family contains five members that form dimers and regulate the transcription of various genes including cytokines, cell adhesion molecules, the pro-proliferative proteins c-*myc* and cyclin D1, and several inhibitors of apoptosis (15). Inhibitors of the NFκB pathway show promise as anticancer and anti-inflammatory agents (16). Parthenolide, a sesquiterpene lactone that was first isolated from the feverfew herb (*Tanacetum parthenium*) native to Central America (17), is a relatively specific small molecule inhibitor of NFκB (18). Parthenolide and other members of the sesquiterpene lactone class have garnered recent attention as promising candidates for cancer treatment either as single agents or in combination with other cytotoxic drugs (19, 20). For example, parthenolide has anti-inflammatory, anticancer, and antiangiogenic properties and has successfully undergone phase I/II clinical trials (21, 22).

Constitutive NFκB activity is widely observed in many tumor types (23), including breast cancer where it is associated with resistance to apoptosis-inducing agents (24). In many tumor lines, autocrine secretion of cytokines and growth factors has recently been implicated in the constitutive activation of NFκB (25). Importantly, NFκB activity also increases in breast cancer cells as they acquire the ability to grow in the absence of estrogen (26, 27). These findings strongly implicate NFκB signaling in the control of breast cancer cell growth and response to antiestrogens.

In this study, we sought to clarify the mechanism by which NFκB up-regulation may affect resistance to Faslodex and determine whether pharmacologic inhibition of NFκB could restore sensitivity to the drug. We show here that in addition to p65/RelA, expression of the upstream regulator NFκB essential modulator/IκB kinase γ (NEMO/IKKγ) is also increased in the resistant cells. The NFκB inhibitor parthenolide efficiently inhibits cell growth and restores sensitivity to Faslodex by synergistically enhancing apoptosis. Our data indicate that inhibition of NFκB may be a successful approach in the treatment of ER-positive breast cancers that have acquired resistance to antiestrogen therapy. NFκB inhibition also may reduce the incidence or delay the onset of antiestrogen resistance. These data provide support for considering the design of clinical studies combining antiestrogens and parthenolide in ER+ breast cancer.

Materials and Methods

Cell Culture and Reagents

MCF-7–derived MCF7/LCC1 and MCF7/LCC9 cells (11, 12) were routinely cultured in phenol red-free improved minimal essential media (IMEM; Biofluids, Rockville, MD) supplemented with 5% charcoal-stripped calf serum (CCS; CCS-IMEM). Cells were maintained in a humidified atmosphere at 37°C and 95% air/5% CO_2. 17β-Estradiol (estradiol, E2) and parthenolide were purchased from Sigma (St. Louis, MO), and ICI 182,780 (ICI, Faslodex) was a kind gift of Dr. Alan Wakeling (AstraZeneca, Macclesfield, Cheshire, United Kingdom).

Cell Lysis, Immunoblotting, and Immunoprecipitation

Cells were grown in either 10-cm^2 dishes or T-75 cm^2 tissue culture flasks before lysis. To determine the effects of parthenolide and ICI 182,780 on protein expression, cells were treated with vehicle, 100 nmol/L ICI 182,780 (the IC_{50} for the control/parental LCC1 cells), or 600 nmol/L parthenolide singly or in combination in CCS-IMEM for 72 hours. Cells were then lysed in modified radioimmunoprecipitation assay buffer [150 mmol/L NaCl, 50 mmol/L Tris (pH 7.5), 1% Igepal CA-630, and 0.5% deoxycholate] supplemented with Complete Mini protease inhibitor cocktail tablets (Roche, Mannheim, Germany) and 1 mmol/L sodium orthovanadate phosphatase inhibitor (Sigma). Lysates were clarified by centrifugation and total protein was quantitated using the bicinchoninic acid assay purchased from Pierce (Rockford, IL). Whole cell lysate (20 μg) was resolved by PAGE using NuPAGE 12% precast gels (Invitrogen, Carlsbad, CA). Proteins were then transferred to nitrocellulose membranes, which were probed with the following antibodies overnight at 4°C: p65 NFκB sc-109 (1:800; Santa Cruz Biotechnology, Santa Cruz, CA), p50 NFκB sc-8414 (1:200; Santa Cruz Biotechnology), p52 NFκB (1:200; Upstate Biotechnology, Charlottesville, VA), IKKγ/NEMO sc-8330 (1:200; Santa Cruz Biotechnology), IκBα sc-371 (1:200; Santa Cruz Biotechnology), phospho-Akt (Ser473; 1:1,000, Cell Signaling, Beverly, MA), or Akt (1:1,000, Cell Signaling). Membranes were then incubated with horseradish peroxidase–conjugated secondary antibodies (Amersham Biosciences, Piscataway, NJ)

for 1 hour at room temperature before enhanced chemiluminescence (Amersham Biosciences) and exposure to film. To confirm equal loading of the gels, membranes were reprobed with antibodies for β-actin (1:5,000; Sigma).

For immunoprecipitations, 400 μg of cell lysate were incubated with 2.5 μL of p65 NFκB antibodies overnight at 4°C with rotation. The following day, 30 μL of Protein A-Sepharose beads (Amersham Biosciences) were added for 1 hour at 4°C to recover the immune complexes, which were then washed twice in modified radioimmunoprecipitation assay buffer, twice in Tris-saline [TN; 50 mmol/L Tris (pH 7.5) and 150 mmol/L NaCl], and resuspended in 2× Laemmli sample buffer before electrophoresis as described above.

Cell Proliferation Assays

MCF7/LCC1 and MCF7/LCC9 cells were seeded at a density of 1 to 2 × 10^4 cells per well in 24-well plates, and 24 hours later were treated with the indicated concentrations of drug in CCS-IMEM. Cells were incubated with the drugs for 7 days, and the media were changed on days 3 and 5. Cells were then trypsinized, resuspended in PBS (Biofluids), and counted using a Z1 Single Coulter Counter (Beckman Coulter, Miami, FL). At least three independent experiments were done in quadruplicate, and data were normalized to vehicle-treated cells. Data are presented as the mean ± SE for a representative experiment.

Transcriptional Reporter Assays

The estrogen response element-containing 3xERE-tk-luc reporter plasmid was purchased from Promega (Madison, WI). MCF7/LCC1 and MCF7/LCC9 cells were seeded into 12-well plates at a density of 7 to 8 × 10^4 cells per well. The following day, cells were transfected with 0.4 μg of luciferase reporter plasmid and 0.1 μg pCMV-*Renilla* (Promega) per well using the FuGENE 6 transfection reagent (Roche, Indianapolis, IN). Three hours post-transfection, media were changed and cells were treated with 100 nmol/L ICI 182,780 and/or 600 nmol/L parthenolide in CCS-IMEM for 24 hours. Subsequently, cells were lysed and activation of the luciferase constructs was measured using the Dual Luciferase Assay Kit (Promega). Luminescence was quantified using a Lumat LB 9501 luminometer (EG&G Berthold, Bundoora VIC, Australia). Luciferase values were normalized to *Renilla* luminescence, and four independent experiments were done each at least in quadruplicate. Data are presented as the mean ± SE for all experiments.

Cell Cycle Assays

Cells (n = 5 × 10^5) were seeded into 10-cm^2 dishes 1 day before treatment with 100 nmol/L ICI 182,780 and/or 600 nmol/L parthenolide in CCS-IMEM for 24 hours. Cells were then analyzed for alterations in cell cycle via fluorescence activated cell sorting, which was done by the Lombardi Comprehensive Cancer Center Flow Cytometry Shared Resource according to the method of Vindelov et al. (28). Data are presented as the mean ± SE for three independent experiments.

Apoptosis Assays

Cells (n = 1 × 10^5) were seeded onto 18 × 18 mm glass coverslips in each well of a 6-well plate in duplicate and the following day were treated with 100 nmol/L ICI 182,780 and/or 600 nmol/L parthenolide in CCS-IMEM for 24 hours. Cells were then fixed with 3.7% formalin in PBS for 20 minutes at room temperature prior to Annexin V and propidium iodide staining using the Vybrant Apoptosis Assay Kit 3 purchased from Vector Laboratories (Burlingame, CA). Coverslips were then mounted on glass slides using VectaShield fluorescence mounting medium (Vector Laboratories). Cells were visualized on a Nikon E600 fluorescence microscope (provided by the Lombardi Comprehensive Cancer Center Microscopy Shared Resource), and several random fields (≥200 cells) were scored per treatment condition. The number of cells stained red (propidium iodide, indicating necrosis) was subtracted from the number of cells stained green (Annexin V-FITC, indicating apoptosis), and subsequently divided by the total number of cells seen by phase-contrast. Data are presented as the percentage of apoptotic cells and represent the mean ± SE for three independent experiments.

Statistical Analyses

Two-tailed Student's t tests were used for the comparison of two groups for immunoblot, cell proliferation, and apoptosis assays as indicated. For luciferase reporter assays, Dunn's post hoc t test was used to compare all treatment groups following one-way ANOVA. Defining the nature of the interaction between Faslodex and parthenolide was done by determining the R index (RI; ref. 29). RI values were obtained by calculating the expected cell survival (S_{exp}; the product of survival obtained with drug A alone and the survival obtained with drug B alone) and dividing S_{exp} by the observed cell survival in the presence of both drugs (S_{obs}). $S_{exp}/S_{obs} > 1.0$ indicates a synergistic interaction. This method is an appropriate way to define synergy in this case because clinically relevant concentrations of Faslodex are ineffective on cell proliferation or apoptosis in the resistant MCF7/LCC9 cells when given as a single agent (29).

Results

p65/RelA and NEMO/IKKγ Are Up-Regulated in Antiestrogen-Resistant Cells

Our previous studies identified a 2-fold up-regulation of p65/RelA mRNA in Faslodex-resistant MCF7/LCC9 cells by expression microarray analysis (10). To confirm altered expression of p65 at the protein level and to examine other NFκB family members and regulatory molecules, whole cell lysates were prepared from MCF7/LCC9 cells and antiestrogen-sensitive MCF7/LCC1 cells and subjected to SDS-PAGE and immunoblot analysis. Similar to mRNA levels, p65/RelA protein is increased ~2-fold in the MCF7/LCC9 cells (Fig. 1A, P = 0.001). In contrast, expression of the p50 subunit of the NFκB heterodimer (Fig. 1B, P = 0.35) or of p52 NFκB2 (data not shown) is not different between the cell lines.

Transcriptional activity of the p65/p50 heterodimer is modulated by the inhibitor IκB, which is in turn negatively regulated by the IKK complex comprised of IKKα, IKKβ,

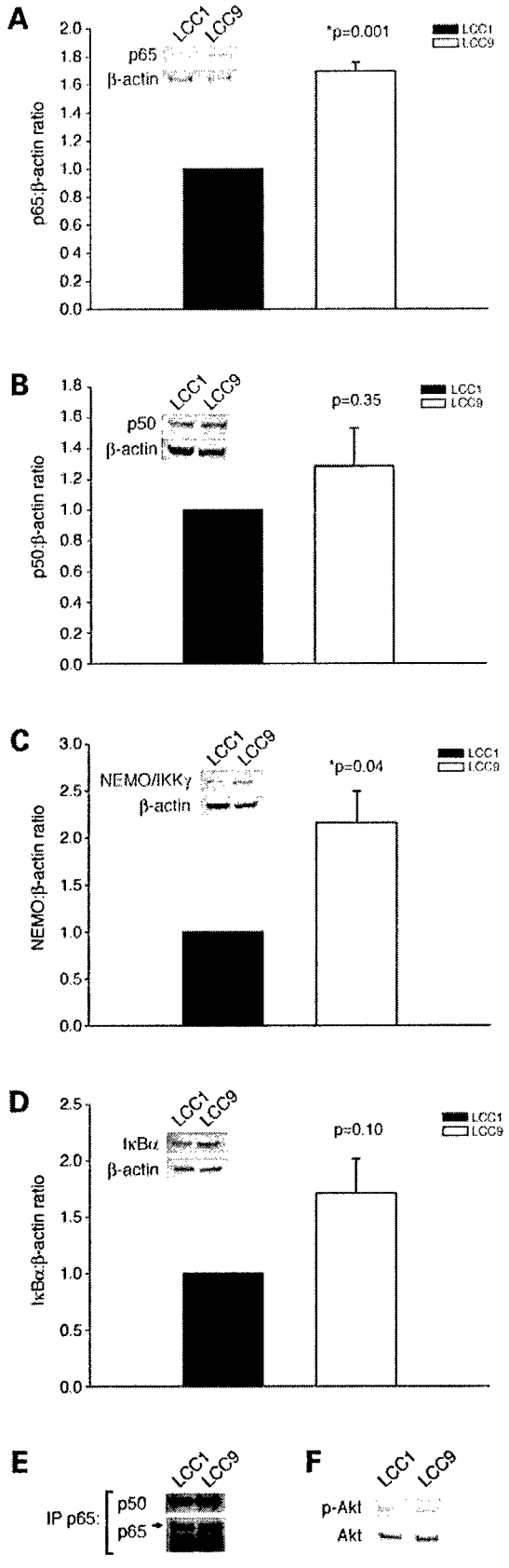

and the scaffolding protein NEMO/IKKγ (30). To determine whether MCF7/LCC9 cells exhibit changes in these regulatory molecules, lysates were immunoblotted for NEMO/IKKγ and IκBα (Fig. 1C and D). Whereas there is no significant change in IκBα expression ($P = 0.10$), a significant 2-fold increase in the level of NEMO/IKKγ is apparent in MCF7/LCC9 cells ($P = 0.04$). NEMO/IKKγ is required for activity of the IKK complex and the inhibitory phosphorylation of IκB in response to inflammatory stimuli that activate NFκB (31), and dysregulation of NEMO is linked to several human pathologies (32). These data suggest that NEMO may also play a role in the response of breast cancer to antiestrogens.

To examine whether the binding of p65 and p50 was altered in antiestrogen-resistant cells, cell lysates were immunoprecipitated with p65 antibodies and immune complexes were captured and subjected to SDS-PAGE as described above (Fig. 1E). No clear differences in p65/p50 complex formation were found between MCF7/LCC1 and MCF7/LCC9 cells.

Independent of the IKK-IκB signaling pathway, NFκB can also be activated by phosphatidylinositol 3-kinase (PI3K); PI3K-mediated activation of Akt can enhance NFκB transcriptional activity without the degradation of IκB (33). Because overexpression of active Akt has also been shown to induce resistance to antiestrogens and cytotoxic drugs (34), MCF7/LCC1 and MCF7/LCC9 cell lysates described above were immunoblotted for phospho-Serine 473 Akt (Fig. 1F). No difference in the level of activated phospho-Akt is observed in the antiestrogen-resistant MCF7/LCC9 cells, suggesting that Akt → NFκB signaling is not the only pathway through which cells can modulate NFκB activation and acquire resistance to Faslodex.

Inhibition of NFκB by Parthenolide Restores Faslodex Sensitivity to MCF7/LCC9 Cells

We have previously reported that MCF7/LCC9 cells are more sensitive than MCF7/LCC1 cells to growth inhibition by parthenolide, suggesting that these cells, in which p65/RelA is up-regulated, are more dependent on NFκB-driven cell growth (10). Faslodex (100 nmol/L) approximates the IC_{50} for proliferation in antiestrogen-sensitive MCF7/LCC1 cells but is ineffective in MCF7/LCC9 cells (Fig. 2A, $P = 0.01$). To determine whether

Figure 1. Expression of NFκB family members and upstream regulatory molecules. **A–D,** quantitiation and representative immunoblots of p65/RelA, p50 NFκB, NEMO/IKKγ, and IκBα levels in MCF7/LCC1 and MCF7/LCC9 cells. Lysates (20 μg) were separated by SDS-PAGE, transferred to nitrocellulose membrane, and immunoblotted. *β-actin,* loading control. *Columns,* mean of at least 3 independent experiments; *bar,* ±SE. *P*s were calculated by Student's *t* test. **E,** coimmunoprecipitation of p65 and p50. Lysates (400 μg) were immunoprecipitated with polyclonal anti-p65 antibodies; immune complexes were isolated and separated by SDS-PAGE, transferred to nitrocellulose, and immunoblotted. **F,** Akt activity is not altered in antiestrogen-resistant MCF7/LCC9 cells. Lysates (20 μg) were separated by SDS-PAGE, transferred to nitrocellulose, and immunoblotted with antibodies specific for phospho-Ser473 of Akt. The membrane was then stripped and reprobed for total Akt.

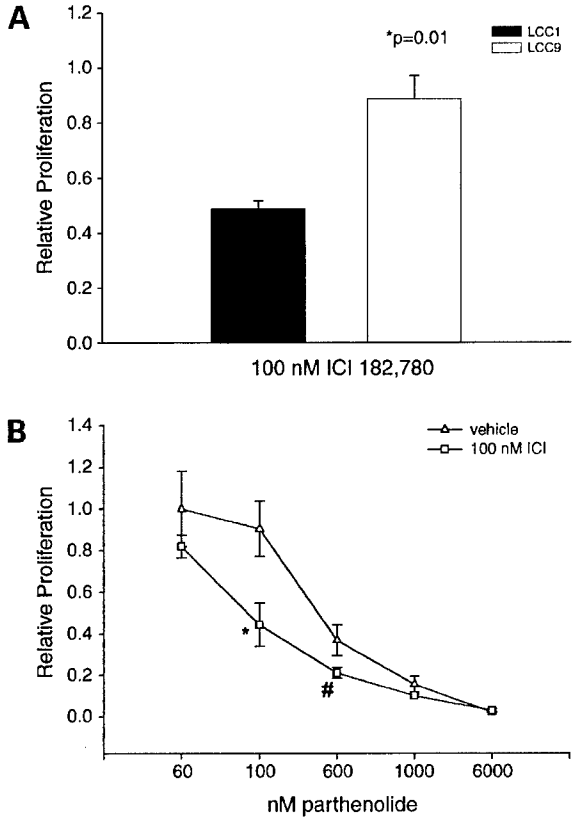

Figure 2. Parthenolide inhibits the proliferation of antiestrogen-resistant cells and partially restores Faslodex sensitivity. **A,** MCF7/LCC9 cells are unresponsive to Faslodex. Cells were seeded in quadruplicate and treated with 100 nmol/L Faslodex in CCS-IMEM for 7 d before counting. *Columns,* mean from a single representative experiment of relative proliferation (relative to vehicle-treated control); *bar,* ±SE. *P* was calculated by Student's *t* test. The experiment was independently done at least thrice. **B,** Faslodex and parthenolide synergistically inhibit MCF7/LCC9 cell proliferation. Cells were seeded in quadruplicate and treated with 0 to 6,000 nmol/L parthenolide in the presence or absence of 100 nmol/L Faslodex in CCS-IMEM for 6 d. *Points,* mean of relative proliferation; *bars,* ±SE. *, $P = 0.034$ versus 100 nmol/L parthenolide without Faslodex by Student's *t* test; RI = 1.82. #, $P = 0.05$ versus 600 nmol/L parthenolide without Faslodex; RI = 1.48.

inhibition of NFκB activity could restore Faslodex sensitivity, MCF7/LCC9 cells were treated with increasing concentrations of parthenolide in the presence or absence of 100 nmol/L Faslodex. In the absence of Faslodex, parthenolide effectively inhibits MCF7/LCC9 cell proliferation with an IC_{50} of 500 to 600 nmol/L. However, the addition of Faslodex generates a significant nearly 5-fold sensitization, where 50% growth inhibition occurs at a concentration of 100 nmol/L parthenolide (Fig. 2B; $P = 0.034$ for parthenolide plus Faslodex compared with parthenolide alone).

The interaction of Faslodex and parthenolide is synergistic in MCF7/LCC9 cells, generating an RI value of 1.82. Treatment with 100 nmol/L Faslodex and 600 nmol/L parthenolide also produces a greater than additive inhibition of cell proliferation ($P = 0.05$, RI = 1.48). These data strongly suggest that the up-regulated NFκB activity present in MCF7/LCC9 cells is a major contributor to the antiestrogen resistance phenotype.

Parthenolide and Faslodex Synergistically Increase Apoptosis

We subsequently sought to define the mechanism by which parthenolide and Faslodex synergistically inhibit the growth of MCF7/LCC9 cells. A primary action of antiestrogens is to antagonize endogenous estrogen and block ER function; Faslodex can achieve this by affecting receptor turnover (5). We asked whether parthenolide can restore Faslodex-mediated inhibition of ER-dependent transcriptional activity (Fig. 3). MCF7/LCC1 and MCF7/LCC9 cells were cotransfected with an ERE-tk-luciferase reporter vector and the pCMV-*Renilla* control vector. Three hours post-transfection, cells were treated with estradiol, Faslodex, and/or parthenolide for 24 hours before performing dual-luciferase promoter-reporter assays.

MCF7/LCC1 cells exhibit a basal ERE-luciferase activity that is enhanced 8-fold by estradiol treatment and almost abolished by Faslodex. In contrast, MCF7/LCC9 cells express a higher basal ERE-luciferase activity that is slightly enhanced by estradiol but is not inhibited by Faslodex treatment. Whereas transcription from an NFκB-dependent reporter is inhibited by 600 nmol/L parthenolide in MCF7/LCC9 cells (data not shown), parthenolide either alone or in combination with Faslodex has no statistically significant effect on ERE-luciferase activity in MCF7/LCC9 cells, suggesting that the mechanism of their antiproliferative synergy does not involve the regulation of ER-dependent transcriptional events.

Treatment with antiestrogens such as Faslodex can have a cytostatic effect on cell growth, typically manifested as

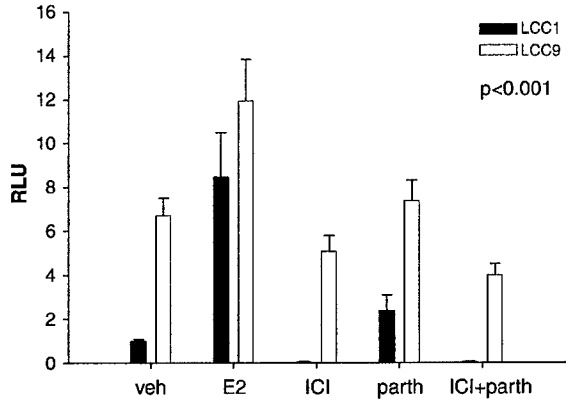

Figure 3. Combined treatment with Faslodex and parthenolide does not inhibit ER-dependent transcriptional activity. MCF7/LCC1 and MCF7/LCC9 cells were transfected in quadruplicate with ERE-tk-luciferase and pCMV-*Renilla* constructs prior to treatment with 10 nmol/L estradiol, 100 nmol/L Faslodex, and 600 nmol/L parthenolide singly or in combination (or ethanol vehicle) in CCS-IMEM for 24 h. *Columns,* mean of the ratio of luciferase-to-Renilla activity (relative light units) for four independent experiments; *bars,* ±SE. $P < 0.001$ for all treatment groups by one-way ANOVA.

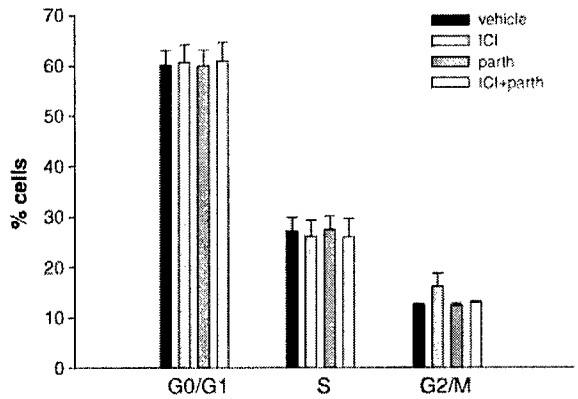

Figure 4. Combined treatment with Faslodex and parthenolide has no effect on the cell cycle profile of MCF7/LCC9 cells. Cells were treated with 100 nmol/L Faslodex, 600 nmol/L parthenolide, Faslodex + parthenolide, or ethanol vehicle in CCS-IMEM for 24 h before cell cycle analysis. *Columns,* mean for three independent experiments (% total cells); *bars,* ±SE.

an accumulation of cells in the G_0-G_1 phase of the cell cycle (1, 8). In some cell systems, parthenolide can arrest cells at the G_2-M phase transition (35). To test whether parthenolide restored the cytostatic activities of Faslodex or induced a G_2-M blockade, MCF7/LCC9 cells were treated with Faslodex ± parthenolide or ethanol vehicle for 24 hours prior to cell cycle analysis (Fig. 4). Parthenolide alone or in combination with Faslodex does not alter the MCF7/LCC9 cell cycle profile, indicating that a block in cell cycle progression does not explain the synergistic reduction in cell growth.

Faslodex and other antiestrogens actively promote apoptosis, and parthenolide has been shown to cooperatively enhance apoptosis induced by other cytotoxic agents such as paclitaxel and 4-hydroxyphenylretinamide (19, 20). Therefore, we measured the effects of Faslodex ± parthenolide or ethanol vehicle on apoptosis as detected by immunostaining for FITC-conjugated Annexin V and propidium iodide staining (Table 1). Approximately 3% of vehicle-treated and 4% of Faslodex-treated MCF7/LCC9 cells undergo apoptosis. In contrast, parthenolide treatment increases the apoptotic fraction to nearly 10%; upon cotreatment with Faslodex and parthenolide, 18% of the cells undergo apoptosis. Importantly, the level of apoptosis seen in the presence of the Faslodex/parthenolide combination was essentially identical to that induced by Faslodex alone in the antiestrogen-sensitive LCC1 cells (Table 1). The strong induction of apoptosis in MCF7/LCC9 cells seen in the presence of both drugs is statistically significant compared with either Faslodex or parthenolide alone ($P = 0.001$ and $P = 0.01$, respectively). The calculated RI = 2.28 for the parthenolide/Faslodex interaction indicates synergistic induction of apoptosis in antiestrogen-resistant MCF7/LCC9 cells.

Parthenolide stabilizes the inhibitor IκB, leading to the retention of p65 in the cytoplasm in an inactive state (36). Therefore, we measured the effects of Faslodex ± parthenolide or ethanol vehicle on IκBα expression (Fig. 5). Since protein levels of IκBα were unchanged in MCF7/LCC9 cells regardless of treatment, parthenolide may be acting through other alternative mechanisms to synergize with Faslodex and restore the apoptotic response to antiestrogen-resistant MCF7/LCC9 cells.

Discussion

Our previous studies reported the p65/RelA subunit of NFκB as being up-regulated in MCF-7–derived MCF7/LCC9 breast cancer cells that had acquired resistance to Faslodex (10, 11). We have now identified additional changes in the expression of NFκB pathway members in these cells and showed that pharmacologic inhibition of NFκB restores Faslodex sensitivity by markedly enhancing apoptosis. Because the NFκB inhibitor parthenolide is currently being investigated in clinical trials (21), these findings have direct clinical relevance and provide support for the design of clinical studies combining antiestrogens and NFκB inhibitors such as parthenolide in ER+ breast cancer.

Protein expression of the p65/RelA subunit of NFκB is increased ~2-fold in MCF7/LCC9 cells when compared with antiestrogen-sensitive MCF7/LCC1 cells; this agrees with the up-regulation in mRNA levels previously observed (10). However, NFκB-dependent transcriptional activity is elevated almost 10-fold in MCF7/LCC9, implying that other elements of the NFκB signaling pathways are activated in these cells. We found no changes in p50 expression or association with p65; there were also no alterations in expression of p52 NFκB2 (data not shown) or the NFκB negative regulator IκBα. PI3K-dependent signaling can also activate NFκB and Akt activation, a primary downstream target of PI3K, has been implicated in antiestrogen resistance. However, we found no differences the levels of phospho-Akt, indicating that this pathway also is unlikely to account for the increased NFκB activity.

In contrast, MCF7/LCC9 cells express ~2-fold higher levels of NEMO/IKKγ. NEMO binds to IKKβ and controls the formation of the IKK complex (37); this is required for the activation of NFκB in response to external stimuli such as tumor necrosis factor α (31, 38). Up-regulation of NEMO

Table 1. Faslodex and parthenolide synergistically enhance apoptosis in MCF7/LCC9 cells

Cell line/drug	% Apoptosis ± SE	*P*
LCC1 vehicle	4.22 ± 0.98	—
LCC1 ICI	19.96 ± 4.43	0.03*
LCC9 vehicle	3.20 ± 1.96	—
LCC9 ICI	4.41 ± 0.90	0.61*
LCC9 parthenolide	9.95 ± 1.21	0.04*
LCC9 ICI + parthenolide	18.34 ± 1.45	0.003*, 0.001†, 0.01‡

NOTE: RI = 2.28 for combination of ICI and parthenolide.
*Versus vehicle.
†Versus ICI.
‡Versus parthenolide.

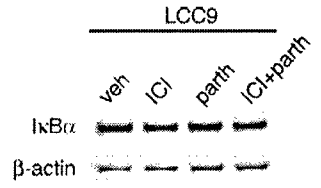

Figure 5. Combined treatment with Faslodex and parthenolide has no effect on the stability of IκBα expression. LCC9 cells were treated with 100 nmol/L Faslodex, 600 nmol/L parthenolide, Faslodex + parthenolide, or ethanol vehicle in CCS-IMEM for 24 h before cell lysis. Lysates (20 μg) were separated by SDS-PAGE, transferred to nitrocellulose membrane, and immunoblotted. *β-actin*, loading control.

in MCF7/LCC9 cells would enhance the kinase activity of IKK and likely adds to the elevated levels of p65 to further increase basal NFκB activation.

Constitutive NFκB activity is known to arise as breast cancer cells progress to an estrogen-independent (26, 27) and antiestrogen-resistant state (10). However, this is the first report implicating NEMO/IKKγ in these events. Regulatory control of NEMO is complex, involving sequential small ubiquitin-like modifier and ubiquitin modification occurring in both the cytoplasm and nucleus (39). Whether the hormonal regulation of NEMO is altered in the MCF7/LCC9 cells has not been determined, but is currently being pursued to clarify further the mechanism by which NFκB activity is elevated in breast cancer cells with acquired antiestrogen resistance.

The NFκB inhibitor parthenolide strongly represses the proliferation of MCF7/LCC9 cells (100 nmol/L, ineffective; IC_{50}= 600 nmol/L) and restores their sensitivity to Faslodex. For example, whereas treatment with 100 nmol/L Faslodex alone is ineffective, 50% growth inhibition is achieved in the presence of only 100 nmol/L parthenolide. This interaction between Faslodex and parthenolide, which generates an estimated RI = 1.82, is synergistic (29). The restoration of Faslodex sensitivity by parthenolide is a significant finding and directly supports our hypothesis that the up-regulated NFκB activity present in MCF7/LCC9 cells is a major contributor to the antiestrogen resistance phenotype.

We have explored several mechanisms through which parthenolide may restore Faslodex sensitivity in antiestrogen-resistant cells. For example, NFκB inhibition could rescue the ability of Faslodex to block ER-dependent transcriptional activity. Expression of several well-characterized estrogen-regulated genes, including *progesterone receptor*, *pS2*, and *cathepsin D* (10), is increased in MCF7/LCC9 cells. This may reflect the 7-fold higher basal levels of ER-dependent transcription in vehicle-treated MCF7/LCC9 cells, relative to that seen in MCF7/LCC1 cells. Faslodex completely inhibits transcription of an ERE-luciferase construct in MCF7/LCC1 cells (antiestrogen sensitive) but has no effect on ERE-mediated transcription in MCF7/LCC9 cells (antiestrogen resistant). Whereas exogenous expression of p65/RelA NFκB can repress ER transcriptional activity *in vitro* (40), treatment with parthenolide does not restore the ability of Faslodex to affect ER transcriptional function in MCF7/LCC9 cells. Thus, the elevated basal ER-dependent transcriptional activity in these cells is likely not due to NFκB up-regulation. Parthenolide may rescue traditional Faslodex-mediated effects in these cells downstream of ER activity and/or in nonclassic ER pathways.

Faslodex induces G_0-G_1 arrest in MCF7/LCC1 cells treated with 100 nmol/L Faslodex (data not shown), but neither Faslodex nor parthenolide has any effect on MCF7/LCC9 cell cycle distribution. Parthenolide-mediated G_2 arrest has been observed at 10-fold higher concentrations than were used in this study (35); therefore, the possibility that MCF7/LCC9 cell cycle progression is inhibited by much higher concentrations of parthenolide cannot be excluded. Indeed, several studies with parthenolide and other sesquiterpene lactones used 1 to 10 μmol/L or greater concentrations to achieve 50% inhibition of cell growth, whereas our cells required up to 10-fold lower concentrations to achieve the same results.

Our results show that the inhibition of cell growth by Faslodex and parthenolide is not primarily cytostatic in nature. In marked contrast, a combination of Faslodex and parthenolide synergistically promotes programmed cell death (RI = 2.28). Importantly, the proportion of apoptotic cells observed in the presence of both drugs (19%) is comparable to that seen when MCF7/LCC1 cells are treated with the same dose of Faslodex (19.9%). Parthenolide can enhance the apoptotic activities of taxanes and retinoids (19, 20), and we now show that it can also potentiate the death of antiestrogen-resistant breast cancer cells by restoring their sensitivity to Faslodex.

DeGraffenried et al. (41) have recently reported that NFκB inhibition by parthenolide increased breast cancer cell sensitivity to tamoxifen. However, these investigators used MCF-7 cells genetically engineered to overexpress activated Akt; these cells exhibit tamoxifen resistance and NFκB activation that is entirely dependent on Akt-mediated pathways. In our cell system, which was derived by selection in the presence of Faslodex rather than by genetic engineering of the cells, NFκB up-regulation does not correlate with enhanced Akt activity.

Sesquiterpene lactones in general, and parthenolide in particular, can prevent the degradation of IκB, block activation of IKK, alkylate cysteine-38 in p65/RelA to prevent DNA binding, and inhibit inducible nitric oxide synthase (36, 42, 43). We found no evidence of IκBα stabilization when MCF7/LCC9 cells were treated with parthenolide either in the absence or presence of Faslodex. Parthenolide can also inhibit p42/44 mitogen-activated protein kinase activity (42) but we observed no reduction in the levels of phospho-mitogen-activated protein kinase in our cells upon parthenolide treatment (data not shown). Interestingly, Nakshatri et al. (44) have recently shown that parthenolide can reverse breast cancer cell resistance to tumor necrosis factor-related apoptosis-inducing ligand by enhancing the activation of c-Jun NH_2-terminal kinase. Whether parthenolide-induced c-Jun NH_2-terminal kinase activity plays a role in its restoration of Faslodex sensitivity in MCF7/LCC9 cells has yet to be determined.

Our studies clearly show that treatment with the NFκB inhibitor parthenolide is a viable approach to restoring Faslodex-induced apoptosis in breast cancer cells that have acquired resistance. Several preclinical studies have shown that parthenolide also is effective in the treatment or chemoprevention of cancer cell growth (45). A phase I study of feverfew in cancer patients was recently completed and reported no significant toxicity observed at the doses tested (21). Other direct or indirect inhibitors of the NFκB pathway also show promise as antiproliferative agents (16) and include some nonsteroidal anti-inflammatory drugs, antioxidants, immunosuppressants, proteasome inhibitors, and glucocorticoids. Our work now shows that inhibition of NFκB may also be useful for the treatment of ER-positive breast cancers that have acquired resistance to antiestrogen therapy, thus restoring the activity of one of the most active and least toxic modalities available in the treatment of endocrine-dependent breast cancer.

References

1. Clarke R, Liu MC, Bouker KB, et al. Antiestrogen resistance in breast cancer and the role of estrogen receptor signaling. Oncogene 2003; 22:7316 – 39.

2. Clarke R, Skaar TC, Bouker KB, et al. Molecular and pharmacological aspects of antiestrogen resistance. J Steroid Biochem Mol Biol 2001;76: 71 – 84.

3. Howell A, DeFriend D, Robertson JFR, Blamey RW, Walton P. Response to a specific antioestrogen (ICI 182,780) in tamoxifen-resistant breast cancer. Lancet 1995;345:29 – 30.

4. Vergote I, Robertson JF. Fulvestrant is an effective and well-tolerated endocrine therapy for postmenopausal women with advanced breast cancer: results from clinical trials. Br J Cancer 2004;90:S11 – 4.

5. Dauvois S, Danielian PS, White R, Parker MG. Antiestrogen ICI 164,384 reduces cellular estrogen receptor content by increasing its turnover. Proc Natl Acad Sci U S A 1992;89:4037 – 41.

6. Fawell SE, White R, Hoare S, Sydenham M, Page M, Parker MG. Inhibition of estrogen receptor-DNA binding by the "pure" antiestrogen ICI 164,384 appears to be mediated by impaired receptor dimerization. Proc Natl Acad Sci U S A 1990;87:6883 – 7.

7. Wakeling AE, Bowler J. Novel antioestrogens without partial agonist activity. J Steroid Biochem 1988;31:645 – 53.

8. Clarke R, Leonessa F, Welch JN, Skaar TC. Cellular and molecular pharmacology of antiestrogen action and resistance. Pharmacol Rev 2001;53:25 – 71.

9. Early Breast Cancer Trialists' Collaborative Group. Tamoxifen for early breast cancer: an overview of the randomized trials. Lancet 1998;351: 1451 – 67.

10. Gu Z, Lee RY, Skaar TC, et al. Association of interferon regulatory factor-1, nucleophosmin, nuclear factor-κB, and cyclic AMP response element binding with acquired resistance to faslodex (ICI 182,780). Cancer Res 2002;62:3428 – 37.

11. Brünner N, Boysen B, Jirus S, et al. MCF7/LCC9: an antiestrogen resistant MCF-7 variant in which acquired resistance to the steroidal antiestrogen ICI 182,780 confers an early crossresistance to the nonsteroidal antiestrogen tamoxifen. Cancer Res 1997;57:3486 – 93.

12. Brünner N, Boulay V, Fojo A, Freter C, Lippman ME, Clarke R. Acquisition of hormone-independent growth in MCF-7 cells is accompanied by increased expression of estrogen-regulated genes but without detectable DNA amplifications. Cancer Res 1993;53:283 – 90.

13. Bouker KB, Skaar TC, Fernandez DR, et al. Interferon regulatory factor-1 mediates the proapoptotic but not cell cycle arrest effects of the steroidal antiestrogen ICI 182,780 (Faslodex, Fulvestrant). Cancer Res 2004;64:4030 – 9.

14. Saura M, Zaragoza C, Bao C, McMillan A, Lowenstein CJ. Interaction of interferon regulatory factor-1 and nuclear factor κB during activation of inducible nitric oxide synthase transcription. J Mol Biol 1999;289:459 – 71.

15. Chen LF, Greene WC. Shaping the nuclear action of NF-κB. Nat Rev Mol Cell Biol 2004;5:392 – 401.

16. Epinat JC, Gilmore TD. Diverse agents act at multiple levels to inhibit the Rel/NF-κB signal transduction pathway. Oncogene 1999;18: 6896 – 909.

17. Bork PM, Schmitz ML, Kuhnt M, Escher C, Heinrich M. Sesquiterpene lactone containing Mexican Indian medicinal plants and pure sesquiterpene lactones as potent inhibitors of transcription factor NF-κB. FEBS Lett 1997;402:85 – 90.

18. Lyss G, Knorre A, Schmidt TJ, Pahl HL, Merfort I. The anti-inflammatory sesquiterpene lactone helenalin inhibits the transcription factor NF-κB by directly targeting p65. J Biol Chem 1998;273: 33508 – 16.

19. Kim DG, You KR, Liu MJ, Choi YK, Won YS. GADD153-mediated anticancer effects of *N*-(4-hydroxyphenyl)retinamide on human hepatoma cells. J Biol Chem 2002;277:38930 – 8.

20. Patel NM, Nozaki S, Shortle NH, et al. Paclitaxel sensitivity of breast cancer cells with constitutively active NF-κB is enhanced by IκBα super-repressor and parthenolide. Oncogene 2000;19:4159 – 69.

21. Curry EA III, Murry DJ, Yoder C, et al. Phase I dose escalation trial of feverfew with standardized doses of parthenolide in patients with cancer. Invest New Drugs 2004;22:299 – 305.

22. Murphy JJ, Heptinstall S, Mitchell JR. Randomised double-blind placebo-controlled trial of feverfew in migraine prevention. Lancet 1988;2:189 – 92.

23. Baldwin AS. Control of oncogenesis and cancer therapy resistance by the transcription factor NF-κB. J Clin Invest 2001; 107:241 – 6.

24. Romieu-Mourez R, Landesman-Bollag E, Seldin DC, Sonenshein GE. Protein kinase CK2 promotes aberrant activation of nuclear factor-κB, transformed phenotype, and survival of breast cancer cells. Cancer Res 2002;62:6770 – 8.

25. Lu T, Sathe SS, Swiatkowski SM, Hampole CV, Stark GR. Secretion of cytokines and growth factors as a general cause of constitutive NFκB activation in cancer. Oncogene 2004;23:2138 – 45.

26. Pratt MAC, Bishop TE, White D, et al. Estrogen withdrawal-induced NF-κB activity and bcl-3 expression in breast cancer cells: roles in growth and hormone independence. Mol Cell Biol 2003;23: 6887 – 900.

27. Nakshatri H, Bhat-Nakshatri P, Martin DA, Goulet RJ, Sledge GW. Constitutive activation of NF-κB during progression of breast cancer to hormone-independent growth. Mol Cell Biol 1997;17:3629 – 39.

28. Vindelov LL, Christensen IJ, Nissen NI. A detergent-trypsin method for the preparation of nuclei for flow cytometric DNA analysis. Cytometry 1983;3:323 – 7.

29. Romanelli S, Perego P, Pratesi G, Carenini N, Tortoreto M, Zunino F. *In vitro* and *in vivo* interaction between cisplatin and topotecan in ovarian carcinoma systems. Cancer Chemother Pharmacol 1998;41:385 – 90.

30. Yamamoto Y, Gaynor RB. IκB kinases: key regulators of the NF-κB pathway. Trends Biochem Sci 2004;29:72 – 9.

31. Tegethoff S, Behlke J, Scheidereit C. Tetrameric oligomerization of IκB kinase γ (IKKγ) is obligatory for IKK complex activity and NF-κB activation. Mol Cell Biol 2003;23:2029 – 41.

32. Smahi A, Courtois G, Rabia SH, et al. The NF-κB signalling pathway in human diseases: from incontinentia pigmenti to ectodermal dysplasias and immune-deficiency syndromes. Hum Mol Genet 2002; 11:2371 – 5.

33. Hatano E, Bennett BL, Manning AM, Qian T, Lemasters JJ, Brenner DA. NF-κB stimulates inducible nitric oxide synthase to protect mouse hepatocytes from TNF-α- and Fas-mediated apoptosis. Gastroenterology 2001;120:1251 – 62.

34. Clark AS, West K, Streicher S, Dennis PA. Constitutive and inducible Akt activity promotes resistance to chemotherapy, trastuzumab, or tamoxifen in breast cancer cells. Mol Cancer Ther 2002;1:707 – 17.

35. Pozarowski P, Halicka DH, Darzynkiewicz Z. Cell cycle effects and caspase-dependent and independent death of HL-60 and Jurkat cells treated with the inhibitor of NF-κB parthenolide. Cell Cycle 2003;2: 377 – 83.

36. Hehner SP, Heinrich M, Bork PM, et al. Sesquiterpene lactones specifically inhibit activation of NF-κB by preventing the degradation of IκB-α and IκB-β. J Biol Chem 1998;273:1288 – 97.

37. May MJ, D'Acquisto F, Madge LA, Glockner J, Pober JS, Ghosh S. Selective inhibition of NF-κB activation by a peptide that blocks the interaction of NEMO with the IκB kinase complex. Science 2000;289: 1550–4.

38. Rudolph D, Yeh WC, Wakeham A, et al. Severe liver degeneration and lack of NF-κB activation in NEMO/IKKγ-deficient mice. Genes Dev 2000; 14:854–62.

39. Hay RT. Modifying NEMO. Nat Cell Biol 2004;6:89–91.

40. McKay LI, Cidlowski JA. Cross-talk between nuclear factor-κB and the steroid hormone receptors: mechanisms of mutual antagonism. Mol Endocrinol 1998;12:45–56.

41. DeGraffenried LA, Chandrasekar B, Friedrichs WE, et al. NF-κB inhibition markedly enhances sensitivity of resistant breast cancer tumor cells to tamoxifen. Ann Oncol 2004;15:885–90.

42. Fiebich BL, Lieb K, Engels S, Heinrich M. Inhibition of LPS-induced p42/44 MAP kinase activation and iNOS/NO synthesis by parthenolide in rat primary microglial cells. J Neuroimmunol 2002; 132:18–24.

43. Garcia-Pineres AJ, Castro V, Mora G, et al. Cysteine 38 in p65/NF-κB plays a crucial role in DNA binding inhibition by sesquiterpene lactones. J Biol Chem 2001;276:39713–20.

44. Nakshatri H, Rice SE, Bhat-Nakshatri P. Antitumor agent parthenolide reverses resistance of breast cancer cells to tumor necrosis factor-related apoptosis-inducing ligand through sustained activation of c-Jun N-terminal kinase. Oncogene 2004;23:7330–44.

45. Ross JJ, Arnason JT, Birnboim HC. Low concentrations of the feverfew component parthenolide inhibit *in vitro* growth of tumor lines in a cytostatic fashion. Planta Med 1999;65:126–9.